



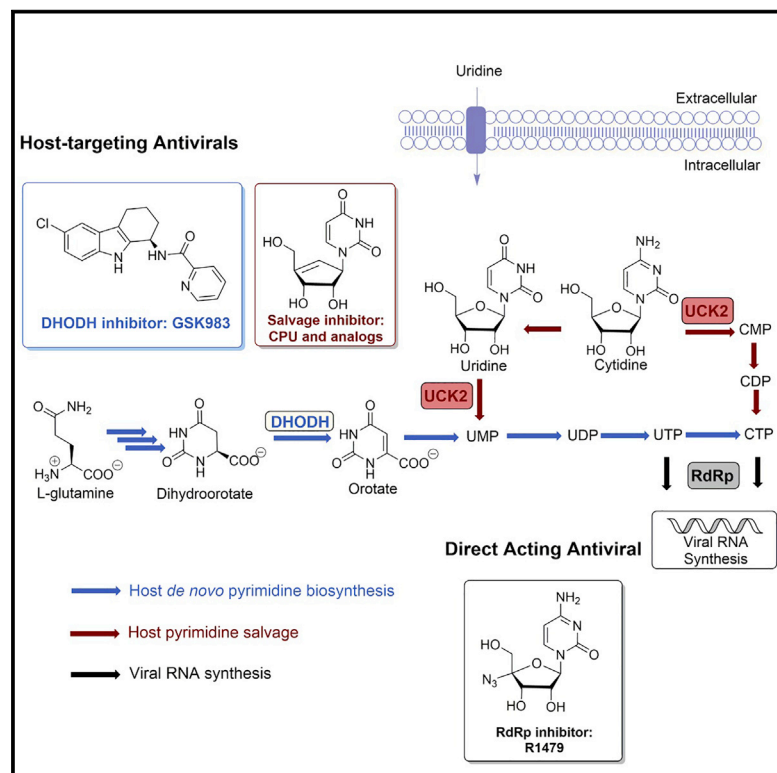
Since January 2020 Elsevier has created a COVID-19 resource centre with free information in English and Mandarin on the novel coronavirus COVID-19. The COVID-19 resource centre is hosted on Elsevier Connect, the company's public news and information website.

Elsevier hereby grants permission to make all its COVID-19-related research that is available on the COVID-19 resource centre - including this research content - immediately available in PubMed Central and other publicly funded repositories, such as the WHO COVID database with rights for unrestricted research re-use and analyses in any form or by any means with acknowledgement of the original source. These permissions are granted for free by Elsevier for as long as the COVID-19 resource centre remains active.

Cell Chemical Biology

Enhancing the Antiviral Efficacy of RNA-Dependent RNA Polymerase Inhibition by Combination with Modulators of Pyrimidine Metabolism

Graphical Abstract



Authors

Qi Liu, Amita Gupta,
Ayse Okesli-Armlovich, ...,
Jan E. Carette, Michael C. Bassik,
Chaitan Khosla

Correspondence

khosla@stanford.edu

In Brief

Many RNA virus infections lack suitable treatments. Liu et al. identified a host-targeting antiviral strategy of modulating pyrimidine metabolism with cyclopentenyl uracil, an inhibitor of pyrimidine salvage, and GSK983, an inhibitor of *de novo* biosynthesis. This combination also increased the potency of an RNA-dependent RNA polymerase inhibitor, against dengue virus.

Highlights

- Cyclopentenyl uracil and analogs inhibit pyrimidine salvage *in vitro* and in cells
- A host-targeting antiviral strategy combining DHODH inhibitors with CPU is explored
- The strategy rescues the antiviral efficacy of a DHODH inhibitor in 20 μM uridine
- Modulating pyrimidine metabolism boosts the antiviral activity of an RdRp inhibitor



Article

Enhancing the Antiviral Efficacy of RNA-Dependent RNA Polymerase Inhibition by Combination with Modulators of Pyrimidine Metabolism

Qi Liu,^{1,2,6,9} Amita Gupta,^{2,3,9} Ayse Okesli-Armlovich,^{1,2,7} Wenjie Qiao,⁴ Curt R. Fischer,^{2,8} Mark Smith,² Jan E. Carette,^{2,4} Michael C. Bassik,^{2,5} and Chaitan Khosla^{1,2,3,10,*}

¹Department of Chemistry, Stanford University, Stanford, CA 94305, USA

²Stanford Chemistry, Engineering and Medicine for Human Health (ChEM-H), Stanford University, Stanford, CA 94305, USA

³Department of Chemical Engineering, Stanford University, Stanford, CA 94305, USA

⁴Department of Microbiology and Immunology, Stanford University, Stanford, CA 94305, USA

⁵Department of Genetics, Stanford University, Stanford, CA 94305, USA

⁶Present address: Abbvie, Sunnyvale, CA 94085, USA

⁷Present address: Gilead Sciences, Foster City, CA 94404, USA

⁸Present address: Octant, Emeryville, CA 94608, USA

⁹These authors contributed equally

¹⁰Lead Contact

*Correspondence: khosla@stanford.edu

<https://doi.org/10.1016/j.chembiol.2020.05.002>

SUMMARY

Genome-wide analysis of the mode of action of GSK983, a potent antiviral agent, led to the identification of dihydroorotate dehydrogenase as its target along with the discovery that genetic knockdown of pyrimidine salvage sensitized cells to GSK983. Because GSK983 is an ineffective antiviral in the presence of physiological uridine concentrations, we explored combining GSK983 with pyrimidine salvage inhibitors. We synthesized and evaluated analogs of cyclopentenyl uracil (CPU), an inhibitor of uridine salvage. We found that CPU was converted into its triphosphate in cells. When combined with GSK983, CPU resulted in large drops in cellular UTP and CTP pools. Consequently, CPU-GSK983 suppressed dengue virus replication in the presence of physiological concentrations of uridine. In addition, the CPU-GSK983 combination markedly enhanced the effect of RNA-dependent RNA polymerase (RdRp) inhibition on viral infection. Our findings highlight a new host-targeting strategy for potentiating the antiviral activity of RdRp inhibitors.

INTRODUCTION

Significant progress in the development of antiviral drugs has been achieved by targeting viral proteins with small molecules (Jordheim et al., 2013; Lou et al., 2014). For example, compounds like aciclovir and zidovudine block viral reverse transcriptase to treat herpes simplex virus and HIV infections, respectively, and RNA-dependent RNA polymerase (RdRp) inhibitors such as dasabuvir and sofosbuvir are used to treat hepatitis C virus infections (Nováková et al., 2018). More recently, the broad-spectrum RdRp inhibitor prodrug remdesivir (Gordon et al., 2020) has received U.S. Food and Drug Administration Emergency Use Authorization for the treatment of coronavirus disease 2019 (COVID-19). Meanwhile, targeting host proteins required for viral propagation is emerging as an attractive alternative that may circumvent the emergence of resistance (Bekerman and Einav, 2015). For example, maraviroc inhibits the human chemokine receptor CCR5, and is therefore used to treat multidrug-resistant HIV (Lieberman-Blum et al., 2008). More recently, pyrimidine biosynthesis has emerged as a potential host-targeting strategy for antivirals (Okesli et al., 2017). Here,

we focus on devising a host-targeting antiviral approach for the treatment of RNA viruses, which cause many serious diseases such as viral hepatitis, influenza, Ebola, dengue, and COVID-19.

In mammalian cells, pyrimidine biosynthesis is a tightly regulated metabolic process. Two complementary pathways—*de novo* biosynthesis and pyrimidine salvage—are responsible for producing UTP and CTP for host as well as viral RNA synthesis (Figure 1). *De novo* pyrimidine biosynthesis is a resource-intensive process. In contrast, salvage occurs via phosphorylation of UMP and CMP derived from intracellular RNA degradation or via facilitated transport and phosphorylation of extracellular uridine, whose plasma concentration is tightly controlled in the low micromolar range (Traut, 1994). Recently, we discovered that GSK983, a broad-spectrum antiviral agent first reported in 2009 (Harvey et al., 2009), is a potent inhibitor of dihydroorotate dehydrogenase (DHODH), a rate-limiting step in *de novo* pyrimidine biosynthesis (Deans et al., 2016). In the course of those unbiased genome-wide studies, we also found that knockdown of uridine/cytidine kinase 2 (UCK2) and uridine monophosphate/cytidine monophosphate kinase 1 (CMPK1) in the pyrimidine



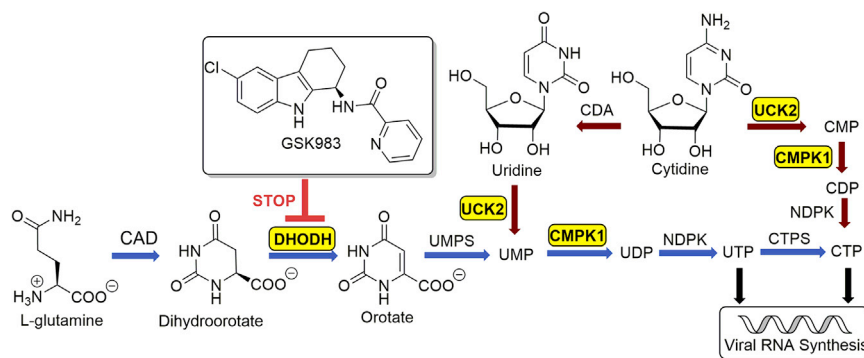


Figure 1. De Novo and Salvage Biosynthesis of Pyrimidine Nucleotides for Host and Viral RNA Synthesis

GSK983 is a DHODH inhibitor. Genes that sensitize cells to GSK983 are highlighted in yellow boxes. Reactions shown with blue arrows comprise the *de novo* biosynthetic pathway, whereas those with red arrows comprise the salvage pathway. CAD, carbamoyl-phosphate synthetase 2, aspartate transcarbamylase, and dihydroorotase; CDA, cytidine deaminase; CMPK1, uridine monophosphate/cytidine monophosphate kinase 1; CTPS, CTP synthetase; DHODH, dihydroorotate dehydrogenase; NDPK, nucleoside diphosphate kinase; UCK2, uridine/cytidine kinase 2; UMPS, uridine monophosphate synthase.

salvage pathway strongly sensitized cells to growth inhibition by GSK983 (Deans et al., 2016). This finding was consistent with the observation that most DHODH inhibitors lack antiviral efficacy *in vivo* despite high potency *in vitro* presumably due to salvage metabolism of circulating uridine by virus-infected cells (Bonavia et al., 2011; Cheung et al., 2017; Grandin et al., 2016; Smee et al., 2012; Wang et al., 2011; Xiong et al., 2020).

To restore the antiviral efficacy of GSK983 in the presence of extracellular uridine, we therefore sought to inhibit pyrimidine salvage. Cyclopentenyl uridine (CPU) is a carbocyclic analog of uridine that has been shown to inhibit human UCK2 (Lim et al., 1984). To our surprise, we learned that the antiviral activity of CPU is due to its remarkable ability to deplete intracellular pyrimidine nucleotide pools via inhibition of salvage biosynthesis pathways. Our findings led us to redirect our search for a fundamentally new type of combination chemotherapy for RNA viruses, as described below.

RESULTS

Diversity-Oriented Syntheses of CPU Analogs

Our search for lead inhibitors of pyrimidine salvage was inspired by earlier reports on the biological activity of CPU and cyclopentenyl cytosine (CPC), which were shown to block uridine salvage *in vitro* and *in vivo* (Cysyk et al., 1995; Lim et al., 1984; Moyer et al., 1985; Schimmel et al., 2007). In these and other reports, CPU was found to be remarkably well tolerated, whereas CPC was considerably more cytotoxic (Blaney et al., 1992; Ford et al., 1991; Song et al., 2001). This contrast is likely due to downstream inhibition of the CTP synthetase by CPC (Schimmel et al., 2007).

Due to the high toxicity of CPC, we undertook structure-activity relationship (SAR) analysis of CPU wherein uracil nucleobase was maintained intact or only modified at the C5 position. Meanwhile, the C-5' substituent of CPU was modified because this is the site of UCK2-catalyzed phosphorylation. In order to rapidly access both nucleobase and carbocyclic moiety analogs, we implemented a diversity-oriented synthetic approach featuring a Mitsunobu reaction as the strategic transformation (Choi et al., 2012).

We first synthesized CPU analogs with nucleobase modifications (Figure 2A). Mitsunobu reactions between the common cyclopentenyl moiety (**1**) (Choi et al., 2004) and the benzoyl protected uracil, C(5)-fluoro-uracil, C(5)-iodo-uracil or thymine

(**2a–2d**) (Racine et al., 2014) furnished the carbon skeleton of C-5 analogs. Removal of acetal, benzoyl, and *tert*-butyldiphenyl silyl (TBDPS) groups then delivered CPU (**4a**) and analogs **4b–4d**.

Next, we turned to synthesis of CPU analogs modified at the C5' position of the cyclopentenyl moiety (Figure 2B). Selective deprotection of TBDPS with tetra-*n*-butylammonium fluoride revealed the primary hydroxyl group (Song et al., 2001), which was then methylated in the presence of Ag₂O (Francisco et al., 2001) to afford the protected 5'-methoxy-CPU. Alternatively, the alcohol could be converted to a terminal fluoride with diethylamino sulfurotrifluoride (Moon et al., 2004), resulting in protected 5'-fluoro CPU. Mesylation or acetylation of **5**, followed by NaN₃ substitution (Schaudt and Blechert, 2003) or Pd(OH)₂/C-catalyzed hydrogenation (Bianco et al., 1989) afforded the protected 5'-azido- and 5'-deoxy-CPU, respectively. The resulting protected intermediates were treated with methanolic ammonia and/or HCl to provide analogs **6, 7, 9**, and **11**.

Enzymatic Analysis of CPU Analogs Against UCK2 and CMPK1

In order to guide our SAR studies, we developed an enzymatic assay to evaluate the inhibitory effect of each CPU analog against recombinant human UCK2, which was expressed and purified in *Escherichia coli*. A continuous assay system was optimized by coupling UCK2 activity to the pyruvate kinase reaction, which in turn was coupled to lactate dehydrogenase (Tomoike et al., 2017). Overall reaction progress was continuously monitored by detecting the UV absorption change at 340 nm, which was correlated with the ATP consumption by UCK2.

The effect of 250 μM of each CPU analog on UCK2 activity was evaluated in the presence of 50 μM uridine. CPU and 5-F-CPU showed much higher ATP consumption compared with other analogs (Figure 3A) even after the 50 μM uridine was presumably exhausted, suggesting these two compounds were substrates of UCK2. We then individually measured the steady-state kinetic parameters of UCK2 using uridine, CPU, and 5-F-CPU as substrates. Their *K_M* values were 86, 25, and 41 μM, and their *k_{cat}*/*K_M* values were 2.6 × 10⁵, 1.5 × 10⁵, and 7.3 × 10⁴ s⁻¹ · M⁻¹ (Figure 3B). As predicted by the relative magnitude of these kinetic parameters, addition of CPU or 5-F-CPU to an assay mixture containing UCK2, uridine, and ATP resulted in a dose-dependent decrease in the rate of UMP synthesis (Figure 3C).

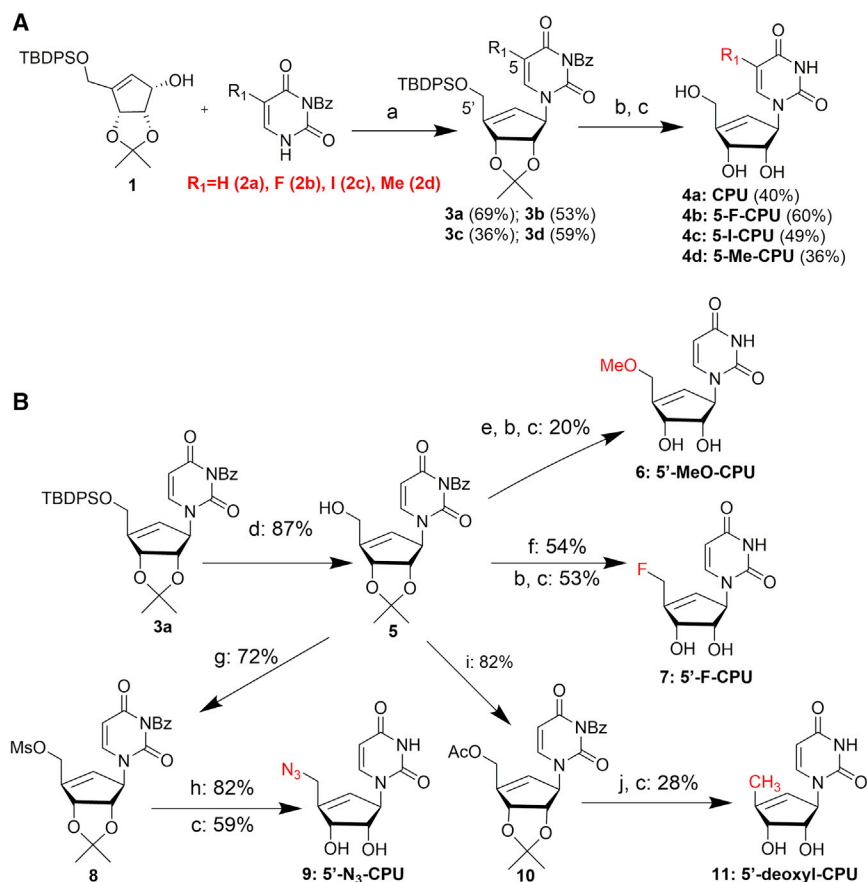


Figure 2. Diversity-Oriented Syntheses of CPU Analogs

(A) Synthesis of CPU (**4a**) and uracil moiety analogs **4b–4d**.

(B) Modification of the C5' position to furnish carbocyclic moiety analogs **6**, **7**, **9**, and **11**.
 (a) DEAD, PPh₃, THF; (b) NH₃, MeOH; (c) HCl, THF; (d) TBAF, THF; (e) Ag₂O, MeI, acetone; (f) DAST, CH₂Cl₂; (g) MsCl, Et₃N, CH₂Cl₂; (h) NaN₃, DMF; (i) AcCl, CH₂Cl₂; (j) Pd(OH)₂, cyclohexene, ethanol. Ac, acetyl; Bz, benzoyl; DAST, diethylaminosulfur trifluoride; DEAD, diethyl azodicarboxylate; Ms, methanesulfonyl; TBAF, tetra-*n*-butylammonium fluoride; TBDPS, *tert*-butyldiphenyl silyl; THF, tetrahydrofuran.

washing (Figure S3) (Martano et al., 2014). LC-MS/MS of nucleotides (Table S1 for MS/MS transitions of selected precursors) was performed using a dynamic multiple reaction monitoring (dMRM) method (Sartain, 2016). Addition of micromolar concentrations of medronic acid into the mobile phase markedly increased the sensitivity for detecting di- and trinucleotides by this method (Hsiao et al., 2018).

With optimized sampling and the analysis method in hand, pyrimidine nucleotide levels were measured in cells cultured with either CPU, 5-F-CPU, or 5'-F-CPU in combination with 1 μM

While CPU and 5-F-CPU were the only UCK2 substrates identified from our panel of carbocyclic nucleoside analogs, some of the other agents had measurable inhibitory activity against this enzyme (Figure 3D). The *K_i* values of the two most potent competitive inhibitors, 5'-F-CPU and 5'-deoxy-CPU, were 170 μM and 230 μM, respectively (Figures 3E and 3F).

Given that CPU and 5-F-CPU could be phosphorylated by UCK2, we sought to establish whether the corresponding monophosphates were substrates of human CMPK1. For this purpose, human CMPK1 was expressed in *E. coli* and purified. We then used recombinant UCK2 to synthesize CMP, CPU-MP, and 5-F-CPU-MP and confirmed their identities by liquid chromatography tandem mass spectrometry (LC-MS/MS) (Figure S1). The results shown in Figure 3G demonstrate that both CPU-MP and 5-F-CPU-MP are substrates of CMPK1, but that the former is a better substrate. Identities of their corresponding products, CPU-DP and 5-F-CPU-DP, were also confirmed by LC-MS/MS (Figure S2).

LC-MS/MS Analysis of Intracellular Nucleotides

To understand the metabolic implications of the above biochemical findings, we developed an LC-MS/MS-based assay that measures the effects of CPU, 5-F-CPU, and 5'-F-CPU on intracellular pyrimidine nucleotide levels. To minimize the perturbation of sample quenching and analysis on the physiological concentrations of these metabolites, we adapted an established protocol for growing cells on glass coverslips to facilitate rapid

GSK983 and 5 μM uridine for 6 h (Figure 4A). Inclusion of CPU or 5-F-CPU led to large decreases in UTP and CTP levels compared with cells treated with GSK983 alone; these effects grew more pronounced at 12 h (Figure S4). CPU depleted UTP and CTP concentrations more strongly than 5-F-CPU. Triphosphates of both CPU and 5-F-CPU could be detected by LC-MS/MS (Figure 4B), suggesting that nucleoside diphosphate kinase, a mammalian enzyme known to have broad substrate scope (Lascu and Gonin, 2000), could convert CPU-DP and 5-F-CPU-DP into their corresponding nucleoside triphosphate analogs. Inclusion of CPU or 5-F-CPU also led to moderate decreases in UMP, CMP, UDP, and CDP levels compared with cells treated with GSK983 alone at both 6 h and 12 h (Figure S4).

Despite its UCK2 inhibitory activity *in vitro*, 5'-F-CPU did not deplete intracellular nucleotide levels and even appeared to increase levels of some intracellular nucleotides (Figures 4A and S4). This contrast suggests that the activity of CPU and 5-F-CPU is derived primarily from their flux through pyrimidine metabolism pathways and not from their inhibition of UCK2.

Antiviral and Cytotoxic Activities of Selected CPU Analogs

From the above enzymological and metabolic data, we hypothesized that the combination of CPU and GSK983 would be more effective at inhibiting dengue virus replication than any other combination. Using an infectious clone of dengue serotype 2 (DENV-2) strain 16681 engineered to express a luciferase

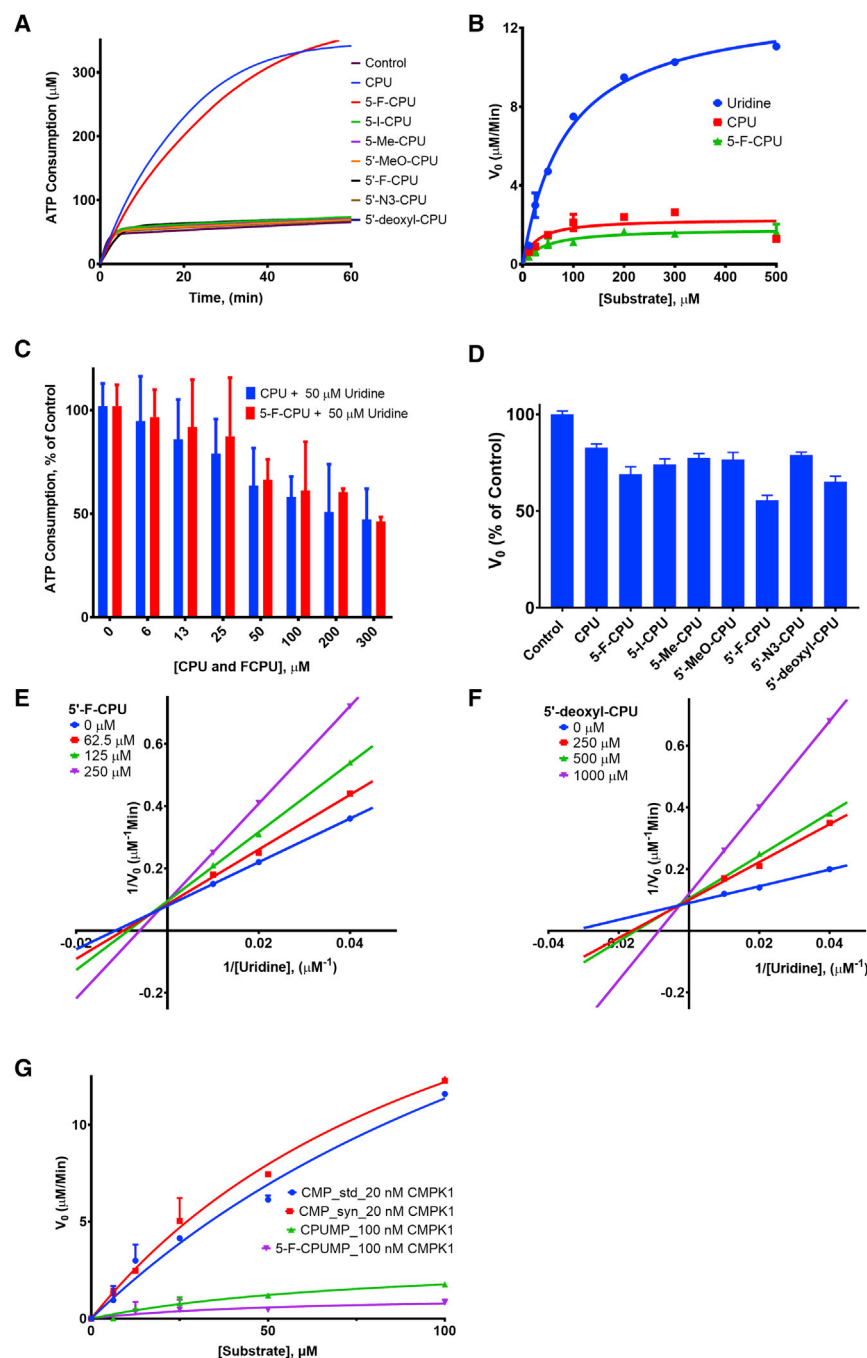


Figure 3. Enzymatic Analysis of CPU Analogs

(A) CPU and 5-F-CPU are UCK2 substrates, as observed by addition of 250 μM of each CPU analog to a UCK2 reaction mixture that also contains 50 μM uridine. All other analogs tested are not UCK2 substrates.

(B) Steady-state kinetic analysis of uridine, CPU, and 5-F-CPU as UCK2 substrates. Error bars represent $\pm\text{SD}$ of three replicates.

(C) Comparative ATP consumption by UCK2 in the presence of 50 μM uridine and varying concentrations of CPU (blue bars) or 5-F-CPU (red bars). Error bars represent $\pm\text{SD}$ of three replicates.

(D) Initial velocities calculated from the data shown in (A).

(E and F) Lineweaver-Burk analysis of 5'-F-CPU (E) and 5'-deoxy-CPU (F) as UCK2 inhibitors.

(G) Comparative activity of CMPK1 on CMP, CPU-MP, and 5-F-CPU-MP. An authentic standard of CMP (std) was tested alongside a UCK2-synthesized sample of the same compound (syn). Error bars represent $\pm\text{SD}$ of three replicates. See also Figures S1 and S2.

However, only CPU appeared to have a workable therapeutic index at this concentration and time point.

To further examine the efficacy and cytotoxicity of CPU, we conducted a more comprehensive checkerboard analysis of the CPU-GSK983 combination. While neither GSK983 nor CPU was effective as a single agent in physiological uridine levels, the combination of both molecules successfully suppressed dengue virus infection (Figure 5B). For example, combining 0.2 μM GSK983 and 250 μM CPU inhibited $\sim 50\%$ of virus replication (Figure 5B). At a CPU dose of 1 mM, virus replication was suppressed almost completely. Notably, the combination treatment had much less effect on A549 cell growth, suggesting that combinations of GSK983 and CPU could be selective for inhibition of virus but not host replication.

To further demonstrate that intracellular nucleotide depletion is correlated with

reporter (Marceau et al., 2016), the efficacy and cytotoxicity of each combination treatment was tested in infected or uninfected cultures of the A549 lung carcinoma cell line (Figure 5A). In all assays, culture medium was supplemented with 20 μM uridine to mimic physiological plasma concentrations. In the presence of 20 μM exogenous uridine, 1 μM of the *de novo* pyrimidine synthesis inhibitor GSK983 alone did not significantly inhibit viral infection or cellular viability (Figure 5A). In line with our original hypothesis, combination of GSK983 with either 500 μM CPU and 5-F-CPU caused significant reductions in viral infection unlike the other cyclopentenyl compounds tested (Figure 5A).

antiviral activity, we also tested the effects of combining GSK983 with a broad inhibitor of nucleoside transport, dipyridamole (DPY). This drug significantly suppressed intracellular nucleotide levels (Figure S4) and consequently inhibited viral replication (Figure S5).

Improving the Therapeutic Index of RdRp Inhibitor R1479 by Combination Treatment Targeting Pyrimidine Biosynthesis

Given that the CPU-GSK983 combination was able to selectively inhibit viral infection through modulation of intracellular

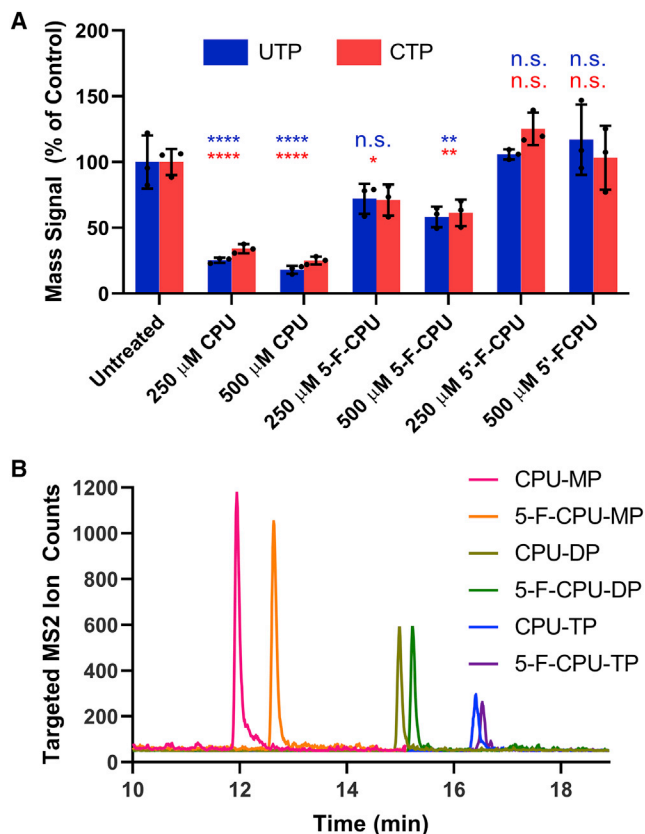


Figure 4. LC-MS/MS Analysis of Intracellular Nucleotides

(A) LC-MS/MS analysis of intracellular uridine and cytidine nucleotide levels after 6 h treatments. In all assays, the culture medium was supplemented with 5 μ M uridine and 1 μ M GSK983. Error bars represent \pm SD of three biological replicates with statistical comparisons with the untreated control denoted for UTP levels (blue) and CTP levels (red) as not significant (n.s.), * $p < 0.05$, ** $p < 0.01$, *** $p < 0.001$, and **** $p < 0.0001$ as calculated by one-way ANOVA, Dunnett's test.

(B) LC-MS/MS detection of mono-, di-, and triphosphates of CPU and 5-F-CPU in cells. The targeted multiple reaction monitoring (MRM) transitions were CPU-MP (319 \rightarrow 79), 5-F-CPU-MP (337 \rightarrow 79), CPU-DP (399 \rightarrow 159), 5-F-CPU-DP (417 \rightarrow 159), CPU-TP (479 \rightarrow 159), and 5-F-CPU-TP (497 \rightarrow 159) as detailed in Table S1.

See also Figures S3 and S4.

nucleotide pools, we hypothesized that the combination should potentiate the effects of an RdRp inhibitor on viral genome replication. Among RdRp inhibitors, the nucleoside inhibitor (NI) class is the largest (Klumpff et al., 2006) and has progressed the furthest in studies against dengue virus (Lim et al., 2015). Many NIs are nucleoside analogs that rely on intracellular phosphorylation to form triphosphate substrates that block RdRp (Sofia et al., 2012). For example, the cytidine analog 4'-azidocytidine (R1479) and its prodrug balapiravir (R1626) have been assessed for treating hepatitis C virus and later dengue virus infections (Chen et al., 2014; Klumpff et al., 2006). However, both compounds failed in clinical trials against dengue due to limited efficacy (Nguyen et al., 2013).

To test whether a combination therapy approach could improve the therapeutic index of R1479, we treated cells with R1479 in combination with GSK983 and CPU. As expected, R1479 showed

dose-dependent inhibition of dengue virus replication with a half-maximal effective concentration (EC_{50}) of $\sim 32 \mu$ M (Figure S6A). Inhibition of either *de novo* or salvage pyrimidine biosynthesis alone did not potentiate the antiviral activity of R1479 or cause additional cytotoxicity (Figure S6A). In contrast, inhibition of both the *de novo* and salvage pathways markedly enhanced the potency of R1479 (Figure 6A). In the presence of 250 μ M CPU, the EC_{50} of R1479 was lowered to $\sim 12 \mu$ M. Notably, such a three-component regimen had minimal impact on the cytotoxicity profile of R1479 (Figure 6B). Regarding other analogs, 5-F-CPU-GSK983 was able to slightly potentiate the antiviral activity of R1479, whereas 5'-F-CPU appeared to actually decrease antiviral efficacy of R1479 (Figures S6B and S6C).

As robust intracellular phosphorylation is critical for both R1479 and CPU activity, we confirmed that competition between these two compounds for intracellular kinases at the rate-limiting mono-phosphorylation step (Ford et al., 1991; Klumpff et al., 2008) should be minimal. Despite its 2'- α -OH group, R1479 is known to be solely phosphorylated by deoxycytidine kinase (dCK) (Klumpff et al., 2008) and was indeed not a UCK2 substrate in our hands (Figure S7). Similarly, cyclopentenyl compounds are substrates of UCK2 and not dCK (Ford et al., 1991).

To gain insight into the mechanism underlying the improvement of R1479 efficacy with CPU, we deployed a replicon assay that bypasses viral entry by electroporation of a reporter DENV-2 RNA construct (Alvarez et al., 2005; Marceau et al., 2016). Such replicon systems include the coding region needed for viral RNA translation and replication, while lacking the structural genes necessary for the production of viral particles. Consequently, viral genome replication is examined independently of viral entry and particle assembly (Kato and Hishiki, 2016). In this assay (Figure 7), the EC_{50} of R1479 alone was $\sim 90 \mu$ M. Inhibition of *de novo* pyrimidine biosynthesis alone with GSK983 did not alter this value ($\sim 96 \mu$ M), whereas addition of 250 μ M CPU shifted it to $\sim 56 \mu$ M. Targeting both the *de novo* and salvage pathways with a combination of 1 μ M GSK and 250 μ M CPU lowered the EC_{50} of R1479 by over 4-fold to $\sim 19 \mu$ M. These results suggest that intracellular nucleotide depletion is the major driver of CPU's antiviral activity. Together, these findings highlight the potential of combining modulators of pyrimidine metabolism with inhibitors of viral genome replication.

DISCUSSION

The flaviviruses, including dengue virus, are an important class of clinically relevant viral pathogens with limited treatment options (Boldescu et al., 2017). In particular, dengue causes hundreds of millions of symptomatic infections annually yet lacks any antiviral treatment, while the sole approved vaccine has limited use because of safety risks associated with vaccination of individuals not previously exposed to dengue (Lim et al., 2013; Sridhar et al., 2018). A series of high-throughput phenotypic cell-based screens have recently identified DHODH inhibition as a potent, broad-spectrum antiviral strategy *in vitro* (Hoffmann et al., 2011; Lucas-Hourani et al., 2013; Luthra et al., 2018; Wang et al., 2011). Furthermore, a DHODH inhibitor was recently shown to suppress SARS-CoV-2 *in vitro* (Xiong et al., 2020). However, DHODH inhibitors lose antiviral activity upon extracellular uridine addition due presumably to pyrimidine salvage

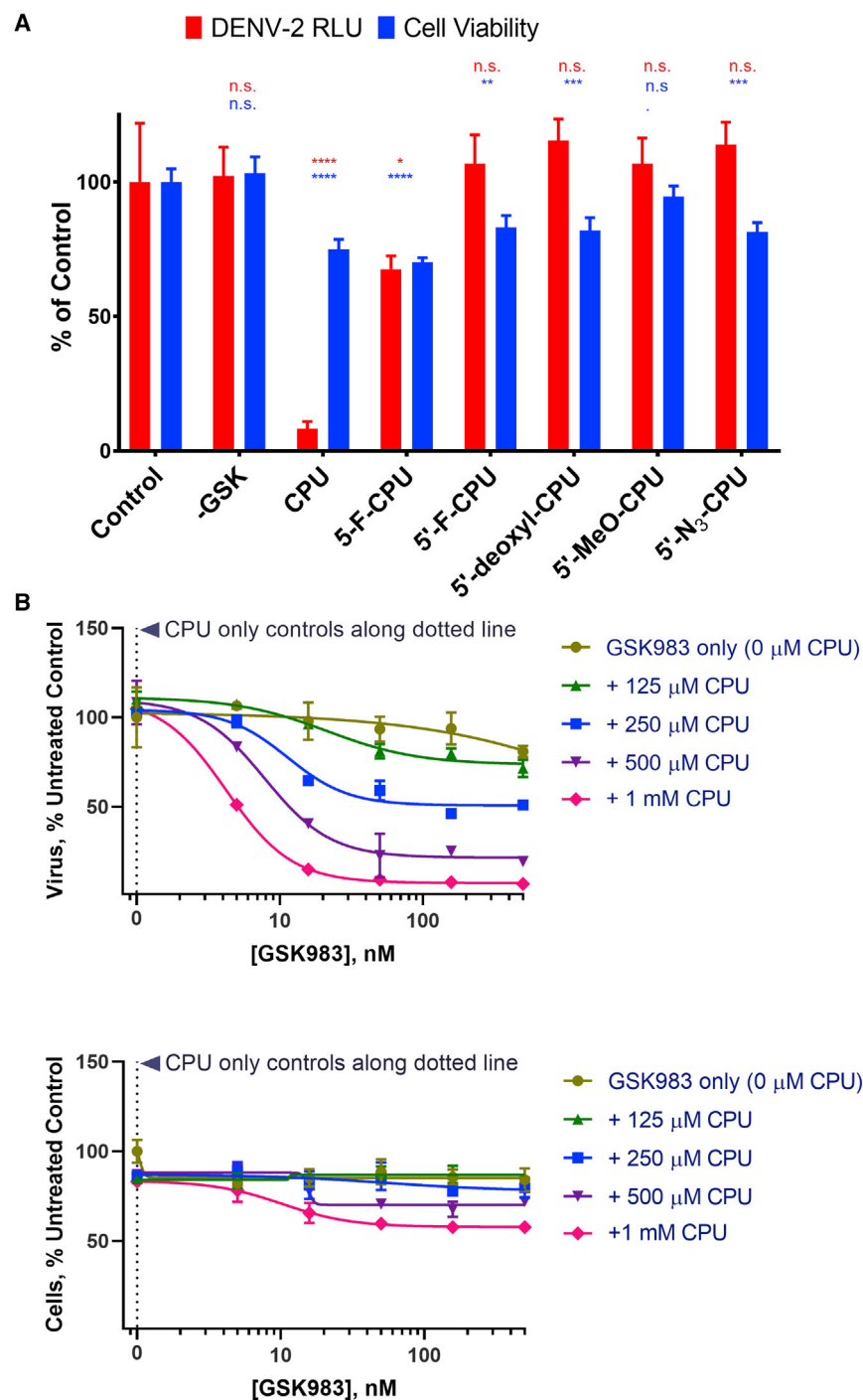


Figure 5. Antiviral and Cytotoxic Activities of Modulators of Pyrimidine Metabolism in the Presence of Exogenous Uridine

(A) Effect of 1 μM GSK983 and 500 μM of individual CPU analogs on luminescence of luciferase-expressing DENV-2 virus (red) and on A549 cell viability (blue) at 72 h, relative to an untreated control. Error bars represent ±SD of three biological replicates with statistical comparisons with the untreated control denoted for viral infection (red) and cell viability (blue) as not significant (n.s.), *p < 0.05, **p < 0.01, ***p < 0.001, and ****p < 0.0001 as calculated by one-way ANOVA, Dunnett's test.

(B) Effects of CPU-GSK983 combination therapy on dengue virus replication and cell proliferation in the presence of exogenous uridine at 48 h. Each GSK983 titration curve is tested in the presence of 0 μM, 125 μM, 250 μM, 500 μM, and 1 mM CPU. Along the dotted line are CPU-only controls at 0 μM, 125 μM, 250 μM, 500 μM, and 1 mM CPU in the absence of GSK983. Error bars represent ±SD of two replicates. RLU, relative light units. See also Figure S5.

synergy between the CPU-GSK983 combination and RdRp inhibition.

Synthesis and evaluation of a series of CPU analogs revealed that CPU and 5-F-CPU were substrates of UCK2, and the resulting monophosphates were substrates of CMPK1. In combination with GSK983, the flux of CPU and 5-F-CPU to their triphosphate forms depleted intracellular pools of pyrimidine NTPs (Figure 4A). As the non-substrate analog 5'-F-CPU did not deplete intracellular pyrimidines despite *in vitro* UCK2 inhibitory activity, our results suggest that CPU's activity in host cells is driven by its ability to block multiple targets in pyrimidine salvage rather than solely UCK2 inhibition.

This distinctive antiviral activity of CPU could conceivably originate from host-targeting modulation of pyrimidine metabolism as well as potential direct-acting antiviral activity of its triphosphate on viral replication. Intracellular nucleotide depletion appears correlated with antiviral activity given that the structurally unrelated nucleoside transport inhibitor DPY

(Deans et al., 2016). While a previous study has explored combining a DHODH inhibitor with guanosine analogs ribavirin or INX-08189 in a non-uridine supplemented cell culture dengue model (Yeo et al., 2015), the antiviral efficacy of a DHODH and a salvage inhibitor has not been previously reported despite interest (Luthra et al., 2018). Here, we found that a GSK983-CPU combination treatment effectively blocked dengue virus replication in the presence of physiological concentrations of extracellular uridine. At the same time, depletion of UTP and CTP led to a

also suppressed intracellular nucleotide levels and viral replication (Figure S5). In addition, while 250 μM CPU in the absence of GSK983 did slightly potentiate the effects of R1479 on viral replication (Figure 7), this did not translate to decreased viral infection at the same time point (Figure S6A). Nevertheless, further investigation of inhibitory effects of CPU-TP on dengue RdRp is warranted. Indeed, as noted previously, NIs are the largest class of RdRp inhibitors (Klump et al., 2008). A multi-factorial approach that incorporates information about

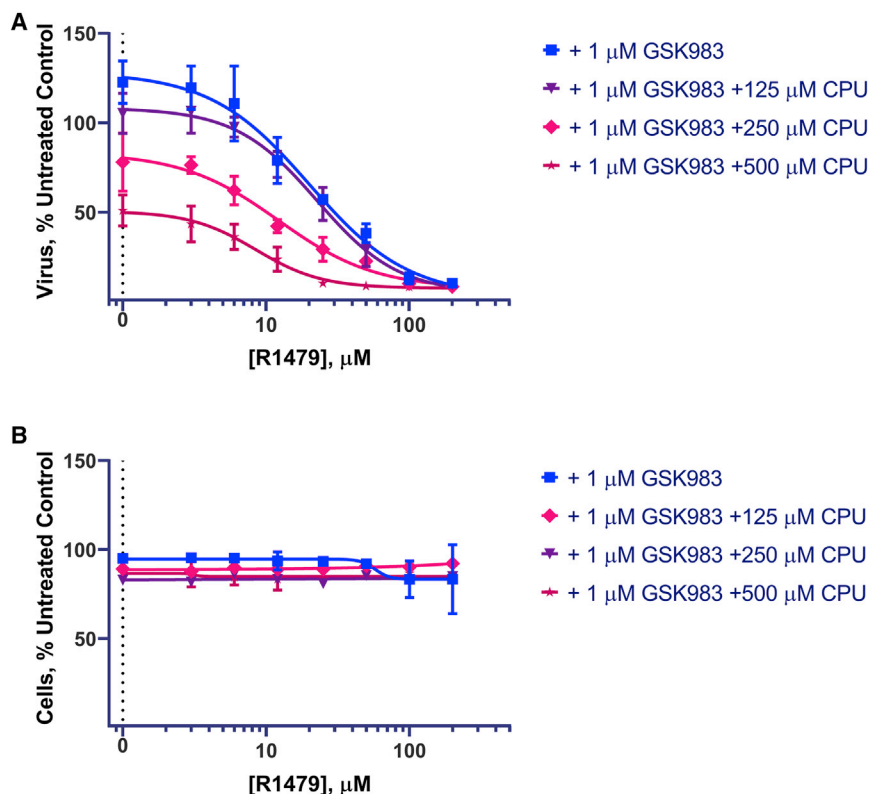


Figure 6. Potentiating the Effects of RdRp Inhibitor R1479 with CPU-GSK983 Combination Treatment

(A) Luminescence of luciferase-expressing DENV-2 virus in A549 cells at 48 h.

(B) Cell viability of A549 cells under the triple combination therapy at 48 h. In all assays, the culture medium was supplemented with 20 μM uridine to mimic plasma uridine concentration and 1 μM GSK983 to block *de novo* pyrimidine biosynthesis. Error bars represent $\pm\text{SD}$ of three replicates.

See also Figures S6 and S7.

interactions with multiple host and viral enzymes will likely be useful for future SAR around CPU as this compound remained the most efficacious in our panel. In addition, efforts to develop specific inhibitors of UCK2 are needed. We previously identified such inhibitors through a high-throughput screen (Okesli-Armlovich et al., 2019); however, these inhibitors appeared to lack sufficient potency to synergize with GSK983 in antiviral models (data not shown).

CPU is known to be safe *in vitro* (Blaney et al., 1992; Ford et al., 1991; Song et al., 2001) and does not show appreciable toxicity in mice (Cysyk et al., 1995) or non-human primates (Blaney et al., 1990). While the safety profile of GSK983 remains less clear, other DHODH inhibitors such as US Food and Drug Administration-approved arthritis drugs leflunomide and teriflunomide and the clinical-stage anti-cancer compound brequinar have been extensively studied in humans and are generally tolerated (Aly et al., 2017). We note that the potential immunosuppressive effects of DHODH inhibitors may be viewed as helpful (Xiong et al., 2020) or harmful (Bonavia et al., 2011) in the treatment of viral infection. Meanwhile, many RdRp inhibitors have been evaluated in clinical trials against dengue. While a preliminary study combining CPU with a *de novo* synthesis inhibitor *in vivo* resulted in toxicity (Cysyk et al., 1995), there is precedent for combining inhibitors of *de novo* pyrimidine synthesis with nucleoside transport inhibitors in humans (Casper et al., 1991). With careful dose optimization and an eye toward immune effects, our results suggest that a combination strategy targeting both host pyrimidine biosynthesis and viral RdRp holds promise as a potential therapy against RNA viruses.

SIGNIFICANCE

RNA virus infections cause serious diseases such as viral hepatitis, influenza, Ebola, dengue, and coronavirus disease 2019, yet many of them lack suitable antiviral treatments. We identified a host-targeting antiviral strategy of modulating pyrimidine metabolism with analogs of cyclopentenyl uracil, an inhibitor of pyrimidine salvage, and GSK983, an inhibitor of *de novo* biosynthesis. This combination therapy also markedly increased the potency of R1479, an RNA-dependent RNA polymerase (RdRp) inhibitor, against dengue virus replication. At efficacious drug doses, the effect on the growth rates of uninfected cells was minimal. In light of the

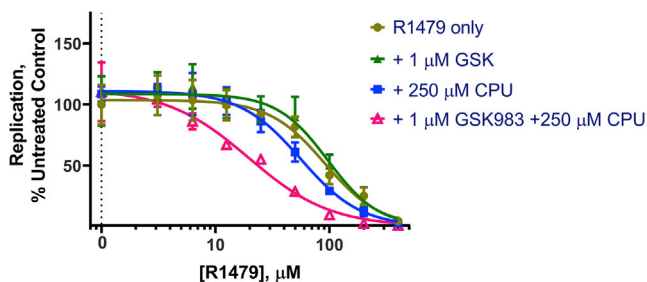


Figure 7. Examining Viral Replication with Combinations of RdRp Inhibitor R1479 with CPU-GSK983 Treatment

Luminescence of luciferase-expressing DENV-2 replicon RNA in A549 cells at 48 h. In all assays, the culture medium was supplemented with 20 μM uridine and 1 μM GSK983. Error bars represent $\pm\text{SD}$ of three replicates.

growing interest in RdRp inhibitors as antiviral agents, our findings shine light on a promising way to enhance their clinical utility by combining them with modulators of mammalian pyrimidine metabolism.

STAR★METHODS

Detailed methods are provided in the online version of this paper and include the following:

- **KEY RESOURCES TABLE**
- **RESOURCE AVAILABILITY**
 - Lead Contact
 - Materials Availability
 - Data and Code Availability
- **EXPERIMENTAL MODELS AND SUBJECT DETAILS**
 - Mammalian Cell Culture
 - Bacterial Cell Culture
 - DENV-Luc Reporter Virus Generation
 - pDENV-Luc Replicon Generation
- **METHOD DETAILS**
 - Synthesis and Characterization of CPU Analogs
 - Purification of Recombinant Human UCK2
 - Purification of Recombinant Human CMPK1
 - *In Vitro* Enzyme Activity Assays with UCK2
 - Enzymatic Synthesis of CMP, CPU-MP, and 5-F-CPU-MP
 - *In Vitro* Enzyme Activity Assays with CMPK1
 - Sample Preparation for LC-MS/MS Analysis
 - LC-MS/MS Analysis
 - DENV-2 Luciferase Reporter Assays
 - Replicon Assays
- **QUANTIFICATION AND STATISTICAL ANALYSIS**

SUPPLEMENTAL INFORMATION

Supplemental Information can be found online at <https://doi.org/10.1016/j.chembiol.2020.05.002>.

ACKNOWLEDGMENTS

The authors wish to thank Roberto Mateo, David Constant, and Khanh Nguyen for helpful discussions and technical advice. The authors also thank Maryline Dong and Nielson Weng for feedback on this manuscript. This research was supported by a grant from the National Institutes of Health (1U19 AI109662 from the National Institute of Allergy and Infectious Diseases) to C.K., M.C.B., and J.E.C. Also, J.E.C. acknowledges NIH (R01 AI141970) for financial support. A.G. is supported by a National Science Foundation Graduate Research Fellowship, a Stanford ChEM-H Chemistry/Biology Interface Pre-doctoral Training Program Fellowship, and an American Research College Scientists (ARCS) Fellowship.

AUTHOR CONTRIBUTIONS

Q.L., A.G., and C.K. designed the research; Q.L., A.G., and W.Q. performed the research investigations; A.O.-A. and C.R.F. aided resource and method development. J.E.C., M.C.B., and C.K. provided supervision and acquired funding. Q.L., A.G., and C.K. wrote the paper (original draft) which was reviewed by all authors. M.S. provided advice.

DECLARATION OF INTERESTS

A patent has been filed on this work by the Stanford University Office of Technology Licensing on behalf of Q.L., A.G., and C.K. with reference label S19-283. M.S. is a paid consultant for Riboscience LLD and Advisory Board Member for Tranquis Therapeutics and Angarus Therapeutics. The other authors declare no competing interests.

Received: September 19, 2019

Revised: March 12, 2020

Accepted: May 4, 2020

Published: May 21, 2020

REFERENCES

- Alvarez, D.E., De Lella Ezcurra, A.L., Fucito, S., and Gamarnik, A.V. (2005). Role of RNA structures present at the 3'UTR of dengue virus on translation, RNA synthesis, and viral replication. *Virology* 339, 200–212.
- Aly, L., Hemmer, B., and Korn, T. (2017). From leflunomide to teriflunomide: drug development and immunosuppressive oral drugs in the treatment of multiple sclerosis. *Curr. Neuropharmacol.* 15, 874–891.
- Bekerman, E., and Einav, S. (2015). Combating emerging viral threats. *Science* 348, 282–283.
- Bianco, A., Passacantilli, P., and Righi, G. (1989). Mild hydrogenolysis process by catalytic transfer hydrogenation. *Tetrahedron Lett* 30, 1405–1408.
- Blaney, S.M., Balis, F.M., Heideman, R.L., McCully, C., Murphy, R.F., Poplack, D.G., Hegedus, L., and Kelley, J.A. (1990). Pharmacokinetics and metabolism of cyclopentenyl cytosine in nonhuman primates. *Cancer Res.* 50, 7915–7919.
- Blaney, S.M., Balis, F.M., Grem, J., Cole, D.E., Adamson, P.C., and Poplack, D.G. (1992). Modulation of the cytotoxic effect of cyclopentenylcytosine by its primary metabolite, cyclopentenyluridine. *Cancer Res.* 52, 3503–3505.
- Boldescu, V., Behnam, M.A.M., Vasilakis, N., and Klein, C.D. (2017). Broad-spectrum agents for flaviviral infections: dengue, Zika and beyond. *Nat. Rev. Drug Discov.* 16, 565–586.
- Bonavia, A., Franti, M., Keaney, E.P., Kuhen, K., Seepersaud, M., Radetich, B., Shao, J., Honda, A., Dewhurst, J., Balabanis, K., et al. (2011). Identification of broad-spectrum antiviral compounds and assessment of the druggability of their target for efficacy against respiratory syncytial virus (RSV). *Proc. Natl. Acad. Sci. U S A* 108, 6739–6744.
- Casper, E.S., Baselga, J., Smart, T.B., Magill, G.B., Markman, M., and Ranhosky, A. (1991). A phase II trial of PALA+dipyridamole in patients with advanced soft-tissue sarcoma. *Cancer Chemother. Pharmacol.* 28, 51–54.
- Chen, Y.-L., Abdul Ghafar, N., Karuna, R., Fu, Y., Lim, S.P., Schul, W., Gu, F., Herve, M., Yokohama, F., Wang, G., et al. (2014). Activation of peripheral blood mononuclear cells by dengue virus infection depotentiates balapiravir. *J. Virol.* 88, 1740–1747.
- Cheung, N.N., Lai, K.K., Dai, J., Kok, K.H., Chen, H., Chan, K.H., Yuen, K.Y., and Tsun Kao, R.Y. (2017). Broad-spectrum inhibition of common respiratory RNA viruses by a pyrimidine synthesis inhibitor with involvement of the host antiviral response. *J. Gen. Virol.* 98, 946–954.
- Choi, W.J., Moon, H.R., Kim, H.O., Yoo, B.N., Lee, J.A., Shin, D.H., and Jeong, L.S. (2004). Preparative and stereoselective synthesis of the versatile intermediate for carbocyclic nucleosides: effects of the bulky protecting groups to enforce facial selectivity. *J. Org. Chem.* 69, 2634–2636.
- Choi, W.J., Chung, H., Chandra, G., Alexander, V., Zhao, L.X., Lee, H.W., Nayak, A., Majik, M.S., Kim, H.O., Kim, J.-H., et al. (2012). Fluorocyclopentenyl-cytosine with broad spectrum and potent antitumor activity. *J. Med. Chem.* 55, 4521–4525.
- Cysyk, R.L., Malinowski, N., Marquez, V., Zaharevitz, D., August, E.M., and Moyer, J.D. (1995). Cyclopentenyl uracil: n effective inhibitor of uridine salvage in vivo. *Biochem. Pharmacol.* 49, 203–207.
- Deans, R.M., Morgens, D.W., Ökesli, A., Pillay, S., Horlbeck, M.A., Kampmann, M., Gilbert, L.A., Li, A., Mateo, R., Smith, M., et al. (2016). Parallel shRNA and CRISPR-Cas9 screens enable antiviral drug target identification. *Nat. Chem. Biol.* 12, 361–366.

- Ford, H., Cooney, D.A., Ahluwalia, G.S., Hao, Z., Rommel, M.E., Hicks, L.R., Dobyms, K.A., and Johns, D.G. (1991). Cellular pharmacology of cyclopentenyl cytosine in Molt-4 lymphoblasts. *Cancer Res.* *51*, 3733–3740.
- Francisco, C.G., Freire, R., González, C.C., León, E.I., Riesco-Fagundo, C., and Suárez, E. (2001). Fragmentation of carbohydrate anomeric alkoxy radicals. synthesis of polyhydroxy piperidines and pyrrolidines related to carbohydrates. *J. Org. Chem.* *66*, 1861–1866.
- Gordon, C.J., Tchesnokov, E.P., Feng, J.Y., Porter, D.P., and Gotte, M. (2020). The antiviral compound remdesivir potently inhibits RNA-dependent RNA polymerase from Middle East respiratory syndrome coronavirus. *J. Biol. Chem.* *295*, 4773–4779.
- Grandin, C., Hourani, M.L., Janin, Y.L., Dauzonne, D., Munier-Lehmann, H., Paturet, A., Taborik, F., Vabret, A., Contamin, H., Tangy, F., et al. (2016). Respiratory syncytial virus infection in macaques is not suppressed by intranasal sprays of pyrimidine biosynthesis inhibitors. *Antivir. Res.* *125*, 58–62.
- Harvey, R., Brown, K., Zhang, Q., Gartland, M., Walton, L., Talarico, C., Lawrence, W., Selleseth, D., Coffield, N., Leary, J., et al. (2009). GSK983: a novel compound with broad-spectrum antiviral activity. *Antivir. Res.* *82*, 1–11.
- Hierholzer, J.C., and Killington, R.A. (1996). Virus isolation and quantitation. In *Virology Methods Manual*, B.W.J. Mahy and H.O. Kangro, eds. (Academic Press), pp. 25–46.
- Hoffmann, H.H., Kunz, A., Simon, V.A., Palese, P., and Shaw, M.L. (2011). Broad-spectrum antiviral that interferes with de novo pyrimidine biosynthesis. *Proc. Natl. Acad. Sci. U S A* *108*, 5777–5782.
- Hsiao, J.J., Potter, O.G., Chu, T.-W., and Yin, H. (2018). Improved LC/MS methods for the analysis of metal-sensitive analytes using medronic acid as a mobile phase additive. *Anal. Chem.* *90*, 9457–9464.
- Jordheim, L.P., Durantel, D., Zoulim, F., and Dumontet, C. (2013). Advances in the development of nucleoside and nucleotide analogues for cancer and viral diseases. *Nat. Rev. Drug Discov.* *12*, 447–464.
- Kato, F., and Hishiki, T. (2016). Dengue virus reporter replicon is a valuable tool for antiviral drug discovery and analysis of virus replication mechanisms. *Viruses* *8*, 1–11.
- Klumpp, K., Lévêque, V., Le Pogam, S., Ma, H., Jiang, W.R., Kang, H., Granycome, C., Singer, M., Laxton, C., Hang, J.Q., et al. (2006). The novel nucleoside analog R1479 (4'-azidocytidine) is a potent inhibitor of NS5B-dependent RNA synthesis and hepatitis C virus replication in cell culture. *J. Biol. Chem.* *281*, 3793–3799.
- Klumpp, K., Kalayanov, G., Ma, H., Le Pogam, S., Leveque, V., Jiang, W.R., Inocencio, N., De Witte, A., Rajyaguru, S., Tai, E., et al. (2008). 2'-Deoxy-4'-azido nucleoside analogs are highly potent inhibitors of hepatitis C virus replication despite the lack of 2'- α -hydroxyl groups. *J. Biol. Chem.* *283*, 2167–2175.
- Lascu, I., and Gonin, P. (2000). The catalytic mechanism of nucleoside diphosphate kinases. *J. Bioenerg. Biomembr.* *32*, 237–246.
- Lieberman-Blum, S.S., Fung, H.B., and Bandres, J.C. (2008). Maraviroc: a CCR5-receptor antagonist for the treatment of HIV-1 infection. *Clin. Ther.* *30*, 1228–1250.
- Lim, M.I., Moyer, J.D., Cysyk, R.L., and Marquez, V.E. (1984). Cyclopentenyluridine and cyclopentenylcytidine analogues as inhibitors of uridine-cytidine kinase. *J. Med. Chem.* *27*, 1536–1538.
- Lim, S.P., Wang, Q.Y., Noble, C.G., Chen, Y.L., Dong, H., Zou, B., Yokokawa, F., Nilar, S., Smith, P., Beer, D., et al. (2013). Ten years of dengue drug discovery: progress and prospects. *Antivir. Res.* *100*, 500–519.
- Lim, S.P., Noble, C.G., and Shi, P.Y. (2015). The dengue virus NS5 protein as a target for drug discovery. *Antivir. Res.* *119*, 57–67.
- Lou, Z., Sun, Y., and Rao, Z. (2014). Current progress in antiviral strategies. *Trends Pharmacol. Sci.* *35*, 86–102.
- Lucas-Hourani, M., Dauzonne, D., Jorda, P., Cousin, G., Lupan, A., Helyncok, O., Caignard, G., Janvier, G., Andre-Leroux, G., Khiar, S., et al. (2013). Inhibition of pyrimidine biosynthesis pathway suppresses viral growth through innate immunity. *PLoS Pathog.* *9*, 1–18.
- Luthra, P., Naidoo, J., Pietzsch, C.A., De, S., Khadka, S., Anantpadma, M., Williams, C.G., Edwards, M.R., Davey, R.A., Bukreyev, A., et al. (2018). Inhibiting pyrimidine biosynthesis impairs Ebola virus replication through depletion of nucleoside pools and activation of innate immune responses. *Antivir. Res.* *158*, 288–302.
- Marceau, C.D., Puschnik, A.S., Majzoub, K., Ooi, Y.S., Brewer, S.M., Fuchs, G., Swaminathan, K., Mata, M.A., Elias, J.E., Sarnow, P., et al. (2016). Genetic dissection of Flaviviridae host factors through genome-scale CRISPR screens. *Nature* *535*, 159–163.
- Martano, G., Kiefer, P., Christen, P., Kentner, D., Bumann, D., and Vorholt, J.A. (2014). Fast sampling method for mammalian cell metabolic analyses using liquid chromatography–mass spectrometry. *Nat. Protoc.* *10*, 1–11.
- Moon, H.R., Lee, H.J., Kim, K.R., Lee, K.M., Lee, S.K., Kim, H.O., Chun, M.W., and Jeong, L.S. (2004). Synthesis of 5'-substituted fluoro-neplanocin A analogues: importance of a hydrogen bonding donor at 5'-position for the inhibitory activity of S-adenosylhomocysteine hydrolase. *Bioorg. Med. Chem. Lett.* *14*, 5641–5644.
- Moyer, J., Karle, J., Malinowski, N.M., Marquez, V.E., Salam, M., Malspeis, L., and Cysyk, R.L. (1985). Inhibition of uridine kinase and the salvage of uridine by modified pyrimidine nucleosides. *Mol. Pharmacol.* *9*, 454–460.
- Nguyen, N.M., Tran, C.N.B., Phung, L.K., Duong, K.T.H., Huynh, H., Ie, A., Farrar, J., Nguyen, Q.T.H., Tran, H.T., Nguyen, C.V.V., Merson, L., et al. (2013). A randomized, double-blind placebo controlled trial of balapiravir, a polymerase inhibitor, in Adult dengue patients. *J. Infect. Dis.* *207*, 1442–1450.
- Nováková, L., Pavlík, J., Chrenková, L., Martinec, O., and Červený, L. (2018). Current antiviral drugs and their analysis in biological materials – Part II: antivirals against hepatitis and HIV viruses. *J. Pharm. Biomed. Anal.* *147*, 378–399.
- Okesli, A., Khosla, C., and Bassik, M.C. (2017). Human pyrimidine nucleotide biosynthesis as a target for antiviral chemotherapy. *Curr. Opin. Biotechnol.* *48*, 127–134.
- Okesli-Armlovich, A., Gupta, A., Jimenez, M., Auld, D., Liu, Q., Bassik, M.C., and Khosla, C. (2019). Discovery of small molecule inhibitors of human uridine-cytidine kinase 2 by high-throughput screening. *Bioorg. Med. Chem. Lett.* *29*, 2559–2564.
- Racine, S., de Nanteuil, F., Serrano, E., and Waser, J. (2014). Synthesis of (carbo)nucleoside analogues by [3+2] annulation of aminocyclopropanes. *Angew. Chem. Int. Ed.* *53*, 8484–8487.
- Sartan, M. (2016). The Agilent metabolomics dynamic MRM database and method. <https://www.agilent.com/cs/library/technicaloverviews/public/5991-6482EN.pdf%20>.
- Schaudt, M., and Blechert, S. (2003). Total synthesis of (+)-astrophylline. *J. Org. Chem.* *68*, 2913–2920.
- Schimmel, K.J.M., Gelderblom, H., and Guchelaar, H.J. (2007). Cyclopentenyl cytosine (CPEC): an overview of its in vitro and in vivo activity. *Curr. Cancer Drug Targets* *7*, 504–509.
- Smee, D.F., Hurst, B.L., and Day, C.W. (2012). D282, a non-nucleoside inhibitor of influenza virus infection that interferes with de novo pyrimidine biosynthesis. *Antivir. Chem. Chemother.* *22*, 263–272.
- Sofia, M.J., Chang, W., Furman, P.A., Mosley, R.T., and Ross, B.S. (2012). Nucleoside, nucleotide, and non-nucleoside inhibitors of hepatitis C virus NS5B RNA-dependent RNA-polymerase. *J. Med. Chem.* *55*, 2481–2531.
- Song, G.Y., Paul, V., Choo, H., Morrey, J., Sidwell, R.W., Schinazi, R.F., and Chu, C.K. (2001). Enantiomeric synthesis of D- and L-cyclopentenyl nucleosides and their antiviral activity against HIV and West Nile virus. *J. Med. Chem.* *44*, 3985–3993.
- Sridhar, S., Luedtke, A., Langevin, E., Zhu, M., Bonaparte, M., Machabert, T., Savarino, S., Zambrano, B., Moureau, A., Khromava, A., et al. (2018). Effect of dengue serostatus on dengue vaccine safety and efficacy. *N. Engl. J. Med.* *379*, 327–340.
- Tomoike, F., Nakagawa, N., Fukui, K., Yano, T., Kuramitsu, S., and Masui, R. (2017). Indispensable residue for uridine binding in the uridine-cytidine kinase family. *Biochem. Biophys. Rep.* *11*, 93–98.

Traut, T.W. (1994). Physiological concentrations of purines and pyrimidines. *Mol. Cell. Biochem.* 140, 1–22.

Wang, Q.-Y., Bushell, S., Qing, M., Xu, H.Y., Bonavia, A., Nunes, S., Zhou, J., Poh, M.K., Florez de Sessions, P., Niyomrattanakit, P., et al. (2011). Inhibition of dengue virus through suppression of host pyrimidine biosynthesis. *J. Virol.* 85, 6548–6556.

Xiong, R., Zhang, L., Li, S., Sun, Y., Ding, M., Wang, Y., Zhao, Y., Wu, Y., Shang, W., Jiang, X., et al. (2020). Novel and potent inhibitors targeting

DHODH, a rate-limiting enzyme in de novo pyrimidine biosynthesis, are broad-spectrum antiviral against RNA viruses including newly emerged coronavirus SARS-CoV-2. *BioRxiv.* <https://doi.org/10.1101/2020.03.11.983056>.

Yeo, K.L., Chen, Y.L., Xu, H.Y., Dong, H., Wang, Q.Y., Yokokawa, F., and Shi, P.Y. (2015). Synergistic suppression of dengue virus replication using a combination of nucleoside analogs and nucleoside synthesis inhibitors. *Antimicrob. Agents Chemother.* 59, 2086–2093.

STAR★METHODS

KEY RESOURCES TABLE

REAGENTS OR RESOURCES	SOURCE	IDENTIFIER
Bacterial and Virus Strains		
<i>E. coli</i> BL21(DE3)	Thermo Scientific	Cat#EC0014
pDENV-Luc infectious clone	Marceau et al. (2016)	N/A
pDENV-Luc replicon	Marceau et al. (2016)	N/A
Chemicals, Peptides and Recombinant Proteins		
DMEM	Gibco	Cat#11995065
Trypsin/EDTA	Gibco	Cat#25300054
Penicillin-Streptomycin	Gibco	Cat#15140122
Glutamine	Gibco	Cat#25030081
Fetal Bovine Serum	HyClone	Cat#SH30396.03
Electroporation Buffer for replicon	Teknova	Cat#E0399
XbaI Restriction Enzyme	New England BioLabs	Cat#R0145S
Lactate dehydrogenase, porcine heart (LDH)	EMD Millipore	Cat#427211
Pyruvate kinase, rabbit muscle type III (PK)	Sigma-Aldrich	Cat#P9136
Adenosine triphosphate disodium trihydrate (ATP)	VMR Life Science	Cat#0220
β -Nicotinamide adenine dinucleotide, reduced disodium salt hydrate (NADH)	Santa Cruz	Cat# sc-205762A
Phosphoenolpyruvate monopotassium salt (PEP)	Sigma-Aldrich	Cat#P7127
Cytidine 5'-monophosphate disodium salt (CMP)	Sigma-Aldrich	Cat#C1006
Uridine	Sigma-Aldrich	Cat#U3750
LB Broth	Fisher BioReagents	Cat#BP97235
Isopropyl-1-thio- β -D-galactopyranoside (IPTG)	Thermo Fisher Scientific	Cat#R0392
R1479	MedChemExpress	Cat#HY-10444
Dipyridamole (DPY)	MP Biomedicals	Cat#0215372205
D-ribose	Chem Impex	Cat#50494709
Tetrabutylammonium fluoride solution (TBAF), 1.0M	Sigma-Aldrich	Cat#216143
Diethyl azodicarboxylate solution (DEAD), 40 wt. %	Sigma-Aldrich	Cat#563110
Triphenylphosphine (PPh ₃)	Sigma-Aldrich	Cat#T84409
Uracil	Sigma-Aldrich	Cat#U0750
5-Fluorouracil	Sigma-Aldrich	Cat#F6627
Thymine	AK Scientific	Cat#J91030
5-Iodouracil	AK Scientific	Cat#K165
Ammonia, ca. 7N solution in methanol	Sigma-Aldrich	Cat#499145
Silver (I) oxide (Ag ₂ O)	Sigma-Aldrich	Cat#226831
Methyl iodide (MeI)	EMD Millipore	Cat#IX0185
Diethylaminosulfur trifluoride (DAST)	Oakwood	Cat#002323
Methanesulfonyl chloride (MsCl)	Sigma-Aldrich	Cat#471259
Triethylamine (NEt ₃)	Thermo Fisher Scientific	Cat#04885
Acetyl chloride (AcCl)	Sigma-Aldrich	Cat#114189

(Continued on next page)

Continued

REAGENTS OR RESOURCES	SOURCE	IDENTIFIER
Palladium hydroxide on carbon [Pd(OH) ₂ /C], 5 wt. %	Acros Organic	Cat#199620100
Cyclohexene	Sigma-Aldrich	Cat#29240
Sodium azide (NaN ₃)	Sigma-Aldrich	Cat#71289
4-(2-Hydroxyethyl)piperazine-1-ethanesulfonic acid (HEPES)	Fisher BioReagents	Cat#BP310-100
Tris(hydroxymethyl)aminomethane base (Tris)	Fisher BioReagents	Cat#BP152-1
Dithiothreitol (DTT)	Fisher BioReagents	Cat#BP172-25
Magnesium chloride (MgCl ₂)	Fisher Chemical	Cat#M33-500
Potassium chloride (KCl)	Fisher Chemical	Cat#P217-500
Medronic acid (InfinityLab Deactivator Additive)	Agilent	Cat#5191-3940
Adenosine ¹⁵ N ₅ 5'-monophosphate disodium salt	Sigma-Aldrich	Cat#662658
Uridine ¹⁵ N ₂ 5'-monophosphate sodium salt	Sigma-Aldrich	Cat#662666
Critical Commercial Assays		
MEGAscript T7 Transcription Kit	Invitrogen	Cat#AM1334
m7G(5')ppp(5')G RNA Cap Structure Analog	New England BioLabs	Cat#S1404S
CellTiter-Glo	Promega	Cat#G7570
Renilla-Glo	Promega	Cat#E2710
Renilla	Promega	Cat#E2820
Experimental Models: Cell Lines		
A549	ATCC	Cat#CCL-185
Vero E6	ATCC	Cat#CRL-1586
Recombinant DNA		
pET21a-UCK2 expression plasmid	Okesli-Armlovich et al. (2019)	N/A
pET28-CMPK1 expression plasmid	Deans et al. (2016)	N/A
Software		
Prism 8.0	GraphPad	https://www.graphpad.com/scientific-software/prism/
ChemDraw Professional 17.1	PerkinElmer	https://www.perkinelmer.com/category/chemdraw
MNOVA 12.0	Mestrelab	https://mestrelab.com/download_file/mnova-12-0-0/
Other		
Centrifugal Filter Unit	Amicon	Cat#UFC900308
Hi Trap Q anion exchange column	GE Healthcare Life Sciences	Cat#17115301

RESOURCE AVAILABILITY

Lead Contact

Further information and requests for resources and reagents should be directed to and will be fulfilled by the lead contact, Chaitan Khosla (Khosla@stanford.edu)

Materials Availability

This study did not generate any unique biological reagents. Synthesis of CPU and related chemicals is detailed within the manuscript.

Data and Code Availability

This study did not generate any unique datasets or code not available in the manuscript files.

EXPERIMENTAL MODELS AND SUBJECT DETAILS

Mammalian Cell Culture

All mammalian cell lines were maintained in a humidified incubator (37°C, 5% CO₂). A549 cells (male) and Vero E6 cells (female) were obtained from the American Type Culture Collection and cultured in DMEM supplemented with 10% FBS, penicillin/streptomycin, and L-glutamine. Upon reaching 50–75% confluence, cells were detached from the growth surface using a trypsin/EDTA solution prior to analysis. Cells were maintained in logarithmic growth during all biological assays.

Bacterial Cell Culture

BL21(DE3) cells were obtained from ThermoFisher Scientific. Cells were cultured in LB Broth at 37°C with agitation or as required for recombinant protein production.

DENV-Luc Reporter Virus Generation

The design of the pDENV-Luc infectious clone derived from dengue serotype 2 (DENV-2) strain 16681 was detailed previously (Marceau et al., 2016). The plasmid was linearized with XbaI and *in vitro* transcribed into the genomic RNA of DENV-Luc virus using the T7 Megascript Kit (Ambion) in the presence of m7G(5')ppp(5')G RNA Cap Structure Analog (NEB). 5 µg DENV-Luc RNA was electroporated into 2X10⁶ Vero E6 cells. The transfected cells were resuspended in DMEM with 10% FBS and 100 U/ml penicillin-streptomycin and transferred into a T-175 flask incubated at 37 °C with 5% CO₂. Supernatants were collected and replenished with fresh medium every 24 h from day 17 to 24 post-transfection, pooled together, clarified by centrifugation and stored in aliquots at –80°C. The amount of infectious DENV-Luc virus in the stock was titrated using the TCID₅₀ assay and calculated by the Spearman & Kärber algorithm as described previously (Hierholzer and Killington, 1996).

pDENV-Luc Replicon Generation

The plasmid pDENV-Luc replicon containing a Renilla luciferase expressing DENV subgenomic replicon was described previously (Marceau et al., 2016). For *in vitro* transcription, 10 µg of plasmid DNA was linearized using the XbaI restriction enzyme. Replicon RNA was generated using the MEGAscript T7 Transcription Kit in the presence of 5mM m7G(5')ppp(5')G RNA Cap Structure Analogue. For assays, two million A549 cells were washed twice with PBS and re-suspended in electroporation buffer (Teknova, E0399), mixed with 4 µg of purified replicon RNA, and electroporated using Bio-Rad Gene Pulser Xcell electroporator using square wave protocol. Electroporated cells were resuspended in pre-warmed culture medium without antibiotics and seeded as required.

METHOD DETAILS

Synthesis and Characterization of CPU Analogs

Unless otherwise noted, all reactions were performed under an argon atmosphere in flame- or oven- dried glassware. Reaction mixtures were stirred using Teflon-coated magnetic stirrer bars and monitored by thin layer silica gel chromatography (TLC) using 0.25 mm silica gel 60F plates with fluorescent indicator from Merck. Plates were visualized under UV or treated by KMnO₄ stain with gentle heating. Products were purified on an AnaLogix IntelliFlash 280 Flash column chromatography system using the solvent gradients indicated. Anhydrous tetrahydrofuran (THF), dichloromethane (CH₂Cl₂), dimethylformamide (DMF), acetone, and Dimethylsulfoxide (DMSO) were obtained from Acros Organics. Diethyl ether (Et₂O), ethyl acetate (EtOAc), hexanes, and methanol (MeOH) were from Fisher Scientific. DMSO used in bioassays and to prepare biological samples was from Fisher BioReagents. All other reagents were from commercial suppliers and were used as received without additional purification. Samples prepared for biological evaluation were purified via preparative HPLC in a water/acetonitrile (MeCN) gradient containing 0.1% (v/v) trifluoroacetic acid (TFA) using an Agilent 1260 Infinity system equipped with an Agilent Prep-C18 column (21.2 x 250 mm).

NMR spectra were measured on a Varian INOVA 500 (¹H at 500 MHz, ¹³C at 125 MHz), a Varian 400 (¹H at 400 MHz, ¹³C at 100 MHz), or a Varian INOVA 600 MHz (¹H at 600 MHz, ¹³C at 150 MHz) magnetic resonance spectrometer, as noted. ¹H chemical shifts were reported relative to the residual solvent peak (CDCl₃ = 7.26 ppm; CD₃OD = 3.31 ppm) as follows: chemical shift (δ) [multiplicity (s = singlet, brs = broad singlet, d = doublet, t = triplet, q = quartet, dd = doublet of doublet, m = multiplet), coupling constant(s) in Hz, integration]. ¹³C chemical shifts were reported relative to the residual deuterated solvent ¹³C signals (CDCl₃ = 77.16 ppm, CD₃OD = 49.00 ppm) and rounded to one decimal places. Infrared spectra were recorded on a Nicolet iS50 FT/IR Spectrometer at the Stanford Nano Share Facilities and were reported in wavenumbers (cm⁻¹). Optical rotation data were obtained using a JASCO DIP were reported as [α]_D20D (c = grams/100 mL, solvent), where D indicates the sodium D line (589 nm). High resolution mass spectra were obtained on an Agilent 6545 QTOF mass spectrometer at the Metabolic Chemistry Analysis Center at Stanford University. The MNova and ChemDraw softwares aided analytical chemistry analysis.

3-benzoyl-1-((3aS,4R,6aR)-6-((tert-butylidiphenylsilyloxy)methyl)-2,2-dimethyl-3a,6a-dihydro-4H-cyclopenta[d][1,3]dioxol-4-yl)pyrimidine-2,4(1H,3H)-dione (3a)

Compound **1** was prepared in 10 steps from D-ribose according to literature procedures (Choi et al., 2004). To a suspension of **1** (440 mg, 1.04 mmol, 1 equiv.), **2a** (270 mg, 1.25 mmol, 1.2 equiv.), and PPh₃ (410 mg, 1.56 mmol, 1.5 equiv.) in THF (12 mL) at 0 °C was added DEAD solution in toluene (720 µL, 1.5 equiv., 40 w% in toluene). After the addition of DEAD, the reaction mixture turned from a white suspension to a yellow solution, which was slowly warmed up to room temperature and stirred overnight. The

reaction mixture was then concentrated, loaded onto a 12g SiO₂ flash cartridge, and purified with a linear gradient of 20–40% EtOAc in hexanes to afford **3a** (446 mg, 0.72 mmol, 69%) as white powder. [α]_D²⁰ –17.0 (c 1.3, MeOH); IR (film, cm⁻¹): 3071, 2930, 2857, 1748, 1705, 1667, 1441, 1429, 1372, 1234, 1112, 905, 732, 704. ¹H NMR (400 MHz, CDCl₃) δ 7.95 (d, *J* = 7.4 Hz, 1H), 7.71 – 7.61 (m, 6H), 7.53 – 7.47 (m, 2H), 7.45 – 7.42 (m, 2H), 7.41 – 7.34 (m, 4H), 6.91 (d, *J* = 8.1 Hz, 1H), 5.77 (d, *J* = 8.1 Hz, 1H), 5.67 (s, 1H), 5.37 (s, 1H), 5.08 (d, *J* = 5.8 Hz, 1H), 4.60 (d, *J* = 5.8 Hz, 1H), 4.47 (d, *J* = 16.4 Hz, 1H), 4.41 (d, *J* = 16.7 Hz, 1H), 1.34 (s, 3H), 1.29 (s, 3H), 1.10 (s, 9H). ¹³C NMR (100 MHz, CDCl₃) δ 168.8, 162.3, 153.6, 149.8, 141.1, 135.6, 135.6, 135.3, 133.3, 133.1, 131.6, 130.7, 130.1, 129.3, 128.0, 128.0, 120.8, 112.9, 102.4, 84.6, 83.4, 68.4, 61.4, 27.3, 27.0, 25.9, 19.4. HRMS (ESI) *m/z* 623.2574 [(M+H)⁺; calcd for C₃₆H₃₉N₂O₆Si⁺: 623.2572].

1-((1*R*,4*R*,5*S*)-4,5-dihydroxy-3-(hydroxymethyl)cyclopent-2-en-1-yl)pyrimidine-2,4(1*H*,3*H*)-dione (4a)

To compound **3a** (30 mg, 0.048 mmol) was added 0.5 mL 7*N* NH₃ solution in methanol. After 1 h, the reaction solvent was removed under positive N₂ atmosphere and the resulting solid was further dried under high vacuum. The reaction crude was then treated with 30 μ L HCl in 300 μ L THF and stirred overnight. Excess NaHCO₃ was added to neutralize the reaction, followed by the addition of 1 mL MeOH. The resulting suspension was filtered through a short Celite pad, rinsed with MeOH, and concentrated. The resulting crude was then resuspended with 1 mL H₂O and subjected to HPLC purification with a linear gradient of 5–20% MeCN (0.1% TFA) in H₂O (0.1% TFA) on a prep C18 column (Agilent 10 prep-C18 250 \times 21.1 mm). Fractions containing desired product was then combined and lyophilized to afford the final product **4a** (4.6 mg, 0.019 mmol, 40%) as white powder. [α]_D²⁰ –62.8 (c 3.2, MeOH); IR (film, cm⁻¹): 3349 (br), 1667, 1465, 1390, 1258, 1202, 1114. ¹H NMR (500 MHz, CD₃OD) δ 7.42 (d, *J* = 7.9 Hz, 1H), 5.71 (s, 1H), 5.49 (s, 1H), 4.90 (s, 1H), 4.52 (d, *J* = 5.9, 1.2 Hz, 1H), 4.33 – 4.19 (m, 2H), 4.04 (t, *J* = 5.6 Hz, 1H). ¹³C NMR (125 MHz, CD₃OD) δ 166.4, 153.1, 152.1, 143.6, 125.5, 102.8, 78.4, 74.0, 67.4, 60.3. HRMS (ESI) *m/z* 263.0644 [(M+Na)⁺; calcd for C₁₀H₁₂N₂NaO₅⁺: 263.0638].

In a similar manner, compound **1** (360 mg, 0.85 mmol, 1 equiv.) was reacted with **2b** (238 mg, 1.02 mmol, 1.2 equiv.) to afford intermediate **3b** as white powder (288 mg, 0.45 mmol, 53%). Intermediate **3b** (32 mg, 0.05 mmol) was then deprotected to afford **4b** (7.7 mg, 0.03 mmol, 60%) as white powder.

3-benzoyl-1-((3*S*,4*R*,6*R*)-6-((tert-butylidiphenylsilyloxy)methyl)-2,2-dimethyl-3*a*,6*a*-dihydro-4*H*-cyclopenta[d][1,3]dioxol-4-yl)-5-fluoropyrimidine-2,4(1*H*,3*H*)-dione (3b)

[α]_D²⁰ –12.9 (c 1.4, CHCl₃); IR (film, cm⁻¹): 3072, 2932, 2857, 1753, 1712, 1665, 1662, 1448, 1373, 1234, 1106, 1088, 732, 702, 687. ¹H NMR (400 MHz, CDCl₃) δ 7.97 – 7.92 (m, 2H), 7.73 – 7.63 (m, 5H), 7.55 – 7.49 (m, 2H), 7.48 – 7.42 (m, 2H), 7.42 – 7.35 (m, 4H), 7.06 (d, *J* = 5.8 Hz, 1H), 5.68 (brs, 1H), 5.41 (brs, 1H), 5.08 (d, *J* = 5.8 Hz, 1H), 4.59 (dd, *J* = 12.1, 6.4 Hz, 1H), 4.54 – 4.35 (m, 2H), 1.34 (s, 3H), 1.29 (s, 3H), 1.11 (s, 9H). ¹³C NMR (100 MHz, CDCl₃) δ 167.3, 154.3, 148.3, 141.4, 139.0, 135.6, 135.6, 133.2, 133.0, 131.2, 130.8, 130.2, 130.2, 129.4, 129.1, 128.0, 125.5, 125.1, 120.4, 113.0, 84.6, 83.2, 68.3, 61.4, 27.3, 27.0, 25.9, 19.4. ¹⁹F NMR (376 MHz, CDCl₃) δ –163.44 (d, *J* = 5.7 Hz). HRMS (ESI) *m/z* 663.2323 [(M+Na)⁺; calcd for C₃₆H₃₇FN₂O₆SiNa⁺: 663.2297].

1-((1*R*,4*R*,5*S*)-4,5-dihydroxy-3-(hydroxymethyl)cyclopent-2-en-1-yl)-5-fluoropyrimidine-2,4(1*H*,3*H*)-dione (4b)

[α]_D²⁰ –87.8 (c 0.45, MeOH); IR (film, cm⁻¹): 3375 (br), 1696, 1660, 1386, 1242, 1115, 1011. ¹H NMR (400 MHz, CD₃OD) δ 7.60 (d, *J* = 6.6 Hz, 1H), 5.68 (q, *J* = 1.8 Hz, 1H), 5.49 (brs, 1H), 4.52 (d, *J* = 5.6 Hz, 1H), 4.26 (d, *J* = 2.2 Hz, 2H), 4.03 (t, *J* = 5.5 Hz, 1H). ¹³C NMR (100 MHz, CD₃OD) δ 159.54 (d, *J* = 26.1 Hz), 152.64, 151.74, 142.07 (d, *J* = 233.0 Hz), 127.39 (d, *J* = 33.7 Hz), 125.24, 78.17, 73.94, 67.73, 60.26. ¹⁹F NMR (376 MHz, CD₃OD) δ –168.53 (dd, *J* = 6.8, 1.7 Hz). HRMS (ESI) *m/z* 259.0722 [(M+H)⁺; calcd for C₁₀H₁₂FN₂O₅⁺: 259.0725].

In a similar manner, compound **1** (245 mg, 0.58 mmol, 1 equiv.) was reacted with **2c** (238 mg, 0.70 mmol, 1.2 equiv.) to afford intermediate **3c** (160 mg, 0.21 mmol, 36%) as white powder. Intermediate **3c** (40 mg, 0.053 mmol) was then deprotected to afford **4c** (9.6 mg, 0.026 mmol, 49%) as white powder.

3-benzoyl-1-((3*S*,4*R*,6*R*)-6-((tert-butylidiphenylsilyloxy)methyl)-2,2-dimethyl-3*a*,6*a*-dihydro-4*H*-cyclopenta[d][1,3]dioxol-4-yl)-5-iodopyrimidine-2,4(1*H*,3*H*)-dione (3c)

[α]_D²⁰ –45.1 (c 1.3, CHCl₃); IR (film, cm⁻¹): 3071, 2932, 2857, 1749, 1703, 1666, 1608, 1420, 1233, 1112, 703. ¹H NMR (400 MHz, CDCl₃) δ 7.93 – 7.90 (m, 1H), 7.72 – 7.63 (m, 5H), 7.54 – 7.48 (m, 3H), 7.45 – 7.37 (m, 6H), 5.72 (brs, 1H), 5.37 (s, 1H), 5.13 (d, *J* = 5.8 Hz, 1H), 4.62 (d, *J* = 5.8 Hz, 1H), 4.51 – 4.34 (m, 2H), 1.34 (s, 3H), 1.29 (s, 3H), 1.09 (s, 9H). ¹³C NMR (100 MHz, CDCl₃) δ 167.8, 159.1, 154.1, 149.5, 145.8, 135.6, 135.4, 133.1, 133.1, 131.1, 130.7, 130.1, 129.4, 128.0, 128.0, 120.6, 113.0, 84.6, 83.4, 69.2, 68.1, 61.4, 27.3, 27.0, 25.9, 19.5. HRMS (ESI) *m/z* 749.1538 [(M+H)⁺; calcd for C₃₆H₃₈I₂N₂O₆Si⁺: 749.1538].

1-((1*R*,4*R*,5*S*)-4,5-dihydroxy-3-(hydroxymethyl)cyclopent-2-en-1-yl)-5-iodopyrimidine-2,4(1*H*,3*H*)-dione (4c)

[α]_D²⁰ –104.0 (c 0.6, MeOH); IR (film, cm⁻¹): 3370 (br), 1682, 1608, 1424, 1260, 1111. ¹H NMR (400 MHz, CD₃OD) δ 7.78 (s, 1H), 5.70 (q, *J* = 1.8 Hz, 1H), 5.47 (brs, 1H), 4.52 (d, *J* = 5.5 Hz, 1H), 4.33–4.20 (m, *J* = 2.1 Hz, 2H), 4.04 (t, *J* = 5.7 Hz, 1H). ¹³C NMR (100 MHz, CD₃OD) δ 163.0, 152.8, 152.4, 148.0, 125.5, 78.6, 73.9, 68.6, 67.9, 60.0. HRMS (ESI) *m/z* 366.9782 [(M+H)⁺; calcd for C₁₀H₁₂I₂N₂O₅⁺: 366.9785].

In a similar manner, compound **1** (113 mg, 0.27 mmol, 1 equiv.) was reacted with **2d** (74 mg, 0.32 mmol, 1.2 equiv.) to afford intermediate **3d** as white powder (100 mg, 0.16 mmol, 59%). Intermediate **3d** (30 mg, 0.047 mmol) was then deprotected to afford **4d** (4.3 mg, 0.017 mmol, 36%) as white powder.

3-benzoyl-1-((3*S*,4*R*,6*R*)-6-((tert-butylidiphenylsilyloxy)methyl)-2,2-dimethyl-3*a*,6*a*-dihydro-4*H*-cyclopenta[d][1,3]dioxol-4-yl)-5-methylpyrimidine-2,4(1*H*,3*H*)-dione (3d)

[α]_D²⁰ –27.8 (c 1.2, CHCl₃); IR (film, cm⁻¹): 3071, 2932, 2857, 1748, 1699, 1656, 1429, 1371, 1235, 1111, 732, 702. ¹H NMR (500 MHz, CDCl₃) δ 7.97 – 7.89 (m, 2H), 7.71 – 7.61 (m, 5H), 7.53 – 7.46 (m, 3H), 7.45 – 7.42 (m, 1H), 7.40 – 7.35 (m, 4H), 6.90 (brs, 1H), 5.73 (s, 1H), 5.37 (s, 1H), 5.13 (d, *J* = 5.8 Hz, 1H), 4.65 (dd, *J* = 16.3, 4.7 Hz, 1H), 4.47 – 4.37 (m, 2H), 1.96 (s, 3H), 1.34 (s, 3H), 1.29 (s, 3H), 1.09 (s,

9H). ^{13}C NMR (125 MHz, CDCl_3) δ 169.1, 163.0, 152.9, 149.8, 137.2, 135.6, 135.1, 133.2, 133.1, 131.7, 130.6, 130.1, 129.3, 128.0, 121.3, 112.7, 111.0, 84.6, 83.5, 68.3, 61.4, 27.3, 27.0, 25.9, 19.5, 12.8. HRMS (ESI) m/z 637.2734 [(M+H) $^+$]; calcd for $\text{C}_{37}\text{H}_{41}\text{N}_2\text{O}_6\text{Si}^+$: 637.2728].

1-((1R,4R,5S)-4,5-dihydroxy-3-(hydroxymethyl)cyclopent-2-en-1-yl)-5-methylpyrimidine-2,4(1H,3H)-dione (4d)

$[\alpha]_{20}^{\text{D}}$ –78.5 (c 0.38, MeOH); IR (film, cm^{-1}): 3371, 1683, 1476, 1261, 1205, 1114, 1016. ^1H NMR (400 MHz, CD_3OD) δ 7.23 (d, J = 1.2 Hz, 1H), 5.68 (q, J = 1.8 Hz, 1H), 5.48 (brs, 1H), 4.52 (d, J = 5.9 Hz, 1H), 4.26 (q, J = 2.5 Hz, 2H), 4.04 (t, J = 5.6 Hz, 1H), 1.87 (d, J = 1.2 Hz, 3H). ^{13}C NMR (100 MHz, CD_3OD) δ 166.5, 153.3, 151.8, 139.2, 126.0, 111.8, 78.3, 74.0, 67.2, 60.3, 12.3. HRMS (ESI) m/z 277.0799 [(M+Na) $^+$]; calcd for $\text{C}_{11}\text{H}_{14}\text{N}_2\text{O}_5\text{Na}^+$: 277.0795].

3-benzoyl-1-((3aS,4R,6aR)-6-(hydroxymethyl)-2,2-dimethyl-3a,6a-dihydro-4H-cyclopenta[d][1,3]dioxol-4-yl)pyrimidine-2,4(1H,3H)-dione (5)

To a solution of **3a** (300 mg, 0.48 mmol, 1 equiv.) in THF (5 mL) was added TBAF (580 μL , 0.58 mmol, 1.2 equiv., 1 M in THF) at 0 $^\circ\text{C}$. After 2 h, the reaction mixture was quenched with 5 mL of saturated NH_4OH solution and extracted with 5 \times 5 mL EtOAc. The combined organic layers were dried over anhydrous Na_2SO_4 , concentrated, loaded onto a 4 g SiO_2 flash cartridge, and purified with a linear gradient 80–95% EtOAc in hexanes to afford the free primary alcohol **5** (160 mg, 0.42 mmol, 87%) as white powder. $[\alpha]_{20}^{\text{D}}$ –4.9 (c 4.5, CHCl_3); IR (film, cm^{-1}): 3473 (br), 3088, 2988, 2933, 1746, 1702, 1665, 1443, 1374, 1239, 1179, 1239, 1059. ^1H NMR (500 MHz, CDCl_3) δ 7.93 (d, J = 8.4 Hz, 2H), 7.70–7.61 (m, 1H), 7.50 (dd, J = 8.2, 7.4 Hz, 2H), 7.16 (d, J = 8.0 Hz, 1H), 5.81 (d, J = 8.0 Hz, 1H), 5.64 (s, 1H), 5.30 (s, 1H), 5.25 (d, J = 5.8 Hz, 1H), 4.70 (d, J = 5.8 Hz, 1H), 4.43 (d, J = 15.9 Hz, 1H), 4.38 (d, J = 15.9 Hz, 1H), 1.43 (s, 3H), 1.34 (s, 3H). ^{13}C NMR (125 MHz, CDCl_3) δ 168.8, 162.2, 152.5, 149.7, 141.6, 135.3, 131.5, 130.7, 129.3, 121.7, 113.0, 102.5, 84.3, 84.0, 69.2, 60.2, 27.3, 25.8. HRMS (ESI) m/z 385.1391 [(M+H) $^+$]; calcd for $\text{C}_{20}\text{H}_{21}\text{N}_2\text{O}_6^+$: 385.1394].

1-((1R,4R,5S)-4,5-dihydroxy-3-(methoxymethyl)cyclopent-2-en-1-yl)pyrimidine-2,4(1H,3H)-dione (6)

To a solution of **5** (20 mg, 0.05 mmol, 1 equiv.) in dry acetone (0.5 mL) was added Ag_2O (23 mg, 0.1 mmol, 2 equiv.) and MeI (31 μL , 0.5 mmol, 10 equiv.). The reaction mixture was stirred at room temperature for 24 h, filtered through Celite pad, and concentrated in vacuo to afford a residue oil 17 mg. In a similar manner as the synthesis of **3a** from **4a**, the crude was treated with 0.5 mL 7N NH_3 in methanol, followed by 25 μL HCl in 250 μL of THF to furnish the analog **6** (2.5 mg, 0.01 mmol, 20% for three steps). $[\alpha]_{20}^{\text{D}}$ –64.7 (c 0.25, MeOH); IR (film, cm^{-1}): 3369 (br), 2921, 2851, 1682, 1469, 1410, 1262, 1204, 1096. ^1H NMR (600 MHz, CD_3OD) δ 7.40 (d, J = 8.0 Hz, 1H), 5.72 (dd, J = 3.8, 1.7 Hz, 1H), 5.69 (d, J = 8.0 Hz, 1H), 5.51–5.43 (m, 1H), 4.50 (d, J = 5.8 Hz, 1H), 4.14 (ddd, J = 14.1, 2.5, 2.4 Hz, 1H), 4.08 (ddd, J = 14.2, 2.2, 1.8 Hz, 1H), 4.05 (dd, J = 5.7, 5.5 Hz, 1H), 3.40 (s, 3H). ^{13}C NMR (100 MHz, CD_3OD) δ 166.4, 153.0, 148.8, 143.7, 127.5, 102.8, 78.1, 74.0, 70.3, 67.6, 59.0. HRMS (ESI) m/z 277.0799 [(M+Na) $^+$]; calcd for $\text{C}_{11}\text{H}_{14}\text{N}_2\text{O}_5\text{Na}^+$: 277.0795].

3-benzoyl-1-((3aS,4R,6aR)-6-(fluoromethyl)-2,2-dimethyl-3a,6a-dihydro-4H-cyclopenta[d][1,3]dioxol-4-yl)pyrimidine-2,4(1H,3H)-dione (M1)



To alcohol **5** (50 mg, 0.13 mmol, 1 equiv.) in 1 mL CH_2Cl_2 at -78°C was added a stock solution of DAST (0.15 mmol, 1.2 equiv., 200 μL , prepared by diluting 100 μL of DAST with CH_2Cl_2 to 1 mL). The reaction mixture was warmed up to room temperature and stirred overnight before quenching with 1 mL saturated NaHCO_3 . The resulting mixture was then extracted with 3 \times 3 mL EtOAc. The combined organic layers were dried over anhydrous Na_2SO_4 , concentrated, loaded onto a 4 g SiO_2 flash cartridge, and purified with a linear gradient 20–50% EtOAc in hexanes to afford the intermediate **M1** (27 mg, 0.070 mmol, 54%) as white powder. $[\alpha]_{20}^{\text{D}}$ –12.8 (c 2.4, CHCl_3); IR (film, cm^{-1}): 3100, 2989, 2937, 1746, 1704, 1667, 1599, 1441, 1374, 1239, 1179, 1060, 989. ^1H NMR (600 MHz, CDCl_3) δ 7.93 (d, J = 8.1 Hz, 2H), 7.66 (t, J = 7.5 Hz, 1H), 7.51 (dd, J = 7.91, 7.13 Hz, 2H), 7.13 (d, J = 8.1 Hz, 1H), 5.83 (d, J = 8.1 Hz, 1H), 5.72 (s, 1H), 5.32 (s, 1H), 5.26 (d, J = 5.9 Hz, 1H), 5.14 (s, 1H), 5.07 (s, 1H), 4.73 (d, J = 5.7 Hz, 1H), 1.43 (s, 3H), 1.34 (s, 3H). ^{13}C NMR (125 MHz, CDCl_3) δ 168.7, 162.2, 149.6, 141.5, 135.4, 131.5, 130.7, 129.4, 123.2, 113.2, 102.7, 95.7, 84.1, 83.2, 80.5 (d, J = 149 Hz), 78.8, 77.4, 77.2, 76.9, 69.2, 27.3, 25.8. ^{19}F NMR (376 MHz, CDCl_3) δ –224.4 (t, J = 46.5). HRMS (ESI) m/z 387.1366 [(M+H) $^+$]; calcd for $\text{C}_{20}\text{H}_{20}\text{FN}_2\text{O}_5^+$: 387.1351].

1-((1R,4R,5S)-3-(fluoromethyl)-4,5-dihydroxycyclopent-2-en-1-yl)pyrimidine-2,4(1H,3H)-dione (7)

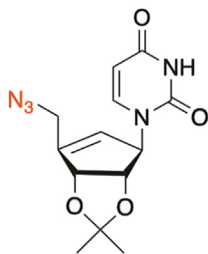
In a similar manner as the synthesis of **4a** from **3a**, compound **M1** (13 mg, 0.034 mmol, 1 equiv.) was treated with 0.5 mL 7N NH_3 in methanol, followed by 25 μL HCl in 250 μL THF to furnish the analog **7** (4.4 mg, 0.018 mmol, 53% for two steps) as white powder. $[\alpha]_{20}^{\text{D}}$ –86.0 (c 0.22, MeOH); IR (film, cm^{-1}): 3365 (br), 2920, 2852, 1675, 1466, 1389, 1265, 1203, 1115. ^1H NMR (600 MHz, CD_3OD) δ 7.42 (d, J = 7.9 Hz, 1H), 5.85 (brs, 1H), 5.70 (d, J = 8.0 Hz, 1H), 5.48 (brs, 1H), 5.15–4.99 (m, 2H), 4.57 (d, J = 6.0 Hz, 1H), 4.10 (dd, J = 6.7, 6.0 Hz, 1H). ^{13}C NMR (150 MHz, CD_3OD) δ 166.2, 152.8, 147.2, 143.6, 128.2, 102.8, 80.5 (d, J = 149 Hz),

77.6, 73.1, 67.4. ^{19}F NMR (376 MHz, CD_3OD) δ - 224.9 (t, J = 46.8 Hz). HRMS (ESI) m/z 265.0592 [(M+Na) $^+$; calcd for $\text{C}_{10}\text{H}_{11}\text{FN}_2\text{O}_4\text{Na}^+$: 265.0595].

1-((3aS,4R,6aR)-4-(3-benzoyl-2,4-dioxo-3,4-dihydropyrimidin-1(2H)-yl)-2,2-dimethyl-3a,6a-dihydro-4H-cyclopenta[d][1,3]dioxol-6-yl)methyl methanesulfonate (8)

To a solution of **5** (60 mg, 0.16 mmol, 1 equiv.) in anhydrous CH_2Cl_2 (2 mL) was added Et_3N (44 μL , 0.32 mmol, 2 equiv.) at 0 $^\circ\text{C}$, followed by the dropwise addition of 0.2 mL MsCl stock solution (0.26 mmol, 1.6 equiv.; Stock solution was prepared by diluting 0.1 mL MsCl with CH_2Cl_2 to 1 mL). After 20 min at 0 $^\circ\text{C}$, the reaction mixture was quenched with 2 mL saturated aqueous solution of NH_4Cl , extracted with 3 \times 3 mL CH_2Cl_2 , dried over anhydrous Na_2SO_4 , concentrated, loaded on a 4g SiO_2 flash cartridge, and purified with a linear gradient 50–95% EtOAc in hexanes to afford the compound **8** (53 mg, 0.11 mmol, 72%) as pale yellow oil. $[\alpha]_{\text{D}}^{20}$ -35.3 (c 2.8, CHCl_3); IR (film, cm^{-1}): 2989, 2937, 1745, 1702, 1661, 1597, 1440, 1354, 1235, 1174, 1087, 959, 906, 729. ^1H NMR (500 MHz, CDCl_3) δ 7.92 (d, J = 7.2 Hz, 2H), 7.66 (dd, J = 8.0, 7.7 Hz, 1H), 7.50 (d, J = 7.8 Hz, 2H), 7.19 (d, J = 8.1 Hz, 1H), 5.83 – 5.67 (m, 2H), 5.30 (d, J = 4.8 Hz, 2H), 4.98 (d, J = 14.0 Hz, 1H), 4.83 (d, J = 14.0 Hz, 1H), 4.71 (d, J = 5.8 Hz, 1H), 3.04 (s, 3H), 1.41 (s, 3H), 1.33 (s, 3H). ^{13}C NMR (125 MHz, CDCl_3) δ 168.7, 162.1, 149.6, 146.3, 141.8, 135.4, 131.4, 130.6, 129.4, 125.9, 113.1, 102.7, 83.8, 83.1, 77.4, 77.2, 76.9, 68.7, 65.0, 38.1, 27.3, 25.7. HRMS (ESI) m/z 463.1185 [(M+H) $^+$; calcd for $\text{C}_{21}\text{H}_{23}\text{N}_2\text{O}_8\text{S}^+$: 463.1170].

1-((3aS,4R,6aR)-6-(azidomethyl)-2,2-dimethyl-3a,6a-dihydro-4H-cyclopenta[d][1,3]dioxol-4-yl)pyrimidine-2,4(1H,3H)-dione (M2)



To the mesylate intermediate **8** (26 mg, 0.056 mmol, 1 equiv.) was added DMF (3 mL) and NaN_3 (80 mg, 1.23 mmol, 22 equiv.). The resulting suspension was heated to 100 $^\circ\text{C}$ and stirred for 18 hours, followed by the addition of 3 mL saturated solution of NH_4Cl . The organic layer was extracted with 3 \times 5 Et_2O , washed with brine, and concentrated under reduced pressure. The crude material was purified through a 4g SiO_2 flash cartridge with a linear gradient 40–95% EtOAc in hexanes to afford the azide intermediate **S2** (14 mg, 0.046 mmol, 82%) as brown oil. $[\alpha]_{\text{D}}^{20}$ -34.0 (c 0.7, CHCl_3); IR (film, cm^{-1}): 3197, 3059, 2988, 2929, 2102, 1687, 1456, 1380, 1243, 1082, 1058. ^1H NMR (500 MHz, CDCl_3) δ 8.78 (brs, 1H), 7.02 (d, J = 8.0 Hz, 1H), 5.71 (d, J = 8.0 Hz, 1H), 5.64 (brs, 1H), 5.31 (brs, 1H), 5.22 (d, J = 5.7 Hz, 1H), 4.65 (d, J = 5.8 Hz, 1H), 4.13 (d, J = 16.0 Hz, 1H), 4.04 (d, J = 16.0 Hz, 1H), 1.44 (s, 3H), 1.35 (s, 3H). ^{13}C NMR (125 MHz, CDCl_3) δ 162.8, 150.5, 150.1, 141.2, 122.1, 112.6, 102.3, 86.2, 84.4, 68.0, 27.4, 26.0, 14.6. HRMS (ESI) m/z 306.1195 [(M+H) $^+$; calcd for $\text{C}_{13}\text{H}_{16}\text{N}_5\text{O}_4^+$: 306.1197].

1-((1R,4R,5S)-3-(azidomethyl)-4,5-dihydroxycyclopent-2-en-1-yl)pyrimidine-2,4(1H,3H)-dione (9)

To intermediate **S2** (6 mg, 0.023 mmol, 1 equiv.) was added THF (250 μL) and concentrated HCl (25 μL). The reaction mixture was stirred at room temperature for 5 h. An excess amount of NaHCO_3 was added to neutralize the reaction, followed by the addition of 1 mL MeOH. The resulting suspension was then filtered through a short Celite pad, rinsed with 2 \times 2 mL MeOH, and concentrated. The resulting crude was resuspended with 1 mL H_2O and subjected to HPLC purification with a linear gradient of 5–20% MeCN (0.1% TFA) in H_2O (0.01% TFA) on a prep C18 column (Agilent 10 prep-C18 250 \times 21.1 mm). Fractions containing the desired product were then combined and lyophilized to afford the final product **9** (3.6 mg, 0.014 mmol, 59%) as white powder. $[\alpha]_{\text{D}}^{20}$ -50.0 (c 0.36, MeOH); IR (film, cm^{-1}): 3358 (br), 2921, 2104, 1683, 1467, 1393, 1261, 1205, 1116. ^1H NMR (400 MHz, CD_3OD) δ 7.39 (d, J = 8.0, 0.6 Hz, 1H), 5.81 (dd, J = 3.2, 1.9 Hz, 1H), 5.70 (d, J = 8.0 Hz, 1H), 5.52 – 5.40 (m, 1H), 4.52 (d, J = 5.8 Hz, 1H), 4.14 – 3.97 (m, 3H). ^{13}C NMR (100 MHz, CD_3OD) δ 166.4, 153.0, 146.7, 143.7, 128.5, 102.9, 77.9, 74.5, 67.9, 50.4. HRMS (ESI) m/z 288.0697 [(M+Na) $^+$; calcd for $\text{C}_{10}\text{H}_{11}\text{N}_5\text{O}_4\text{Na}^+$: 288.0703].

1-((3aS,4R,6aR)-4-(3-benzoyl-2,4-dioxo-3,4-dihydropyrimidin-1(2H)-yl)-2,2-dimethyl-3a,6a-dihydro-4H-cyclopenta[d][1,3]dioxol-6-yl)methyl acetate (10)

Triethylamine (66 μL , 0.48 mmol, 3 equiv.) and acetyl chloride (AcCl) (17 μL , 0.24 mmol, 1.5 equiv.) were sequentially added to a solution of **5** (60 mg, 0.16 mmol, 1 equiv.) in CH_2Cl_2 (2 mL) at 0 $^\circ\text{C}$. The reaction mixture was then warmed up to room temperature and stirred for another hour. A saturated solution of NH_4Cl (2 mL) was added. The organic layer was extracted with 3 \times 3 mL CH_2Cl_2 , washed with H_2O , and concentrated under reduced pressure. The crude material was purified through a 4g SiO_2 flash cartridge with a linear gradient 65–95% EtOAc in hexanes to afford the intermediate **10** (56 mg, 0.13 mmol, 82%) as colorless oil. $[\alpha]_{\text{D}}^{20}$ -62.8 (c 1.3, CHCl_3); IR (film, cm^{-1}): 3080, 2988, 2935, 1742, 1703, 1663, 1599, 1440, 1372, 1236, 1179, 1236, 1058, 904, 731. ^1H NMR (400 MHz, CDCl_3) δ 7.93 (d, J = 7.6 Hz, 2H), 7.78 – 7.61 (m, 1H), 7.50 (dd, J = 8.1, 7.7 Hz, 2H), 7.10 (d, J = 8.1 Hz, 1H), 5.81 (d, J = 8.1 Hz, 1H), 5.61 (brs, 1H), 5.34 (brs, 1H), 5.23 (d, J = 5.7 Hz, 1H), 4.79 (qt, J = 15.0, 1.8 Hz, 2H), 4.67 (d, J = 5.3 Hz, 1H), 2.12 (s, 3H), 1.42 (s, 3H), 1.34 (s, 3H). ^{13}C NMR (100 MHz, CDCl_3) δ 170.7, 168.7, 162.2, 149.7, 148.3, 141.2, 135.3, 131.5, 130.7,

129.3, 123.2, 113.1, 102.6, 84.1, 83.7, 68.6, 60.9, 27.3, 25.9, 20.9. **HRMS** (ESI) m/z 427.1508 [(M+H)⁺; calcd for C₂₂H₂₃N₂O₇⁺: 427.1500].

1-((1R,4R,5S)-4,5-dihydroxy-3-methylcyclopent-2-en-1-yl)pyrimidine-2,4(1H,3H)-dione (11)

To a solution of the allylic acetate **10** (56 mg, 0.13 mmol, 1 equiv.) in 95% ethanol (4 mL) and cyclohexene (2 mL) was added 20 w% Pd(OH)₂ on carbon (20 mg, 1:3 catalyst substrate by weight). The resulting suspension was stirred under reflux overnight. The reaction mixture was then filtered, concentrated, and dried under high vacuum to afford 20 mg crude material as pale-yellow oil. In a similar manner as the preparation of **9**, 6 mg of the crude product was treated with 25 μL HCl in 250 μL THF to afford the final product **11** (8 mg, 0.037 mmol, 28% for two steps) as white solid. [α]_D²⁰ -78.0 (c 0.24, MeOH); **IR** (film, cm⁻¹): 3364 (br), 2921, 2851, 1680, 1468, 1393, 1251, 1203, 1116. **¹H NMR** (400 MHz, CD₃OD) δ 7.39 (d, J = 8.0 Hz, 1H), 5.67 (d, J = 8.0 Hz, 1H), 5.52 – 5.35 (m, 2H), 4.37 (d, J = 5.8 Hz, 1H), 3.99 (dd, J = 5.9, 5.4 Hz, 1H), 1.88 (s, 3H). **¹³C NMR** (100 MHz, MeOH) δ 166.4, 153.1, 148.9, 143.5, 125.6, 102.7, 78.2, 77.2, 68.1, 15.1. **HRMS** (ESI) m/z 247.0685 [(M+Na)⁺; calcd for C₁₀H₁₂N₂O₄Na: 247.0689].

Purification of Recombinant Human UCK2

Previously, human UCK2 was cloned into the pET21a(+) vector resulting in an expression vector for C-terminally 6×His-tagged UCK2 (Okesli-Armlovich et al., 2019). As previously described, *E. coli* BL21(DE3) cells were electroporated with this pET21a-UCK2 expression plasmid, recovered and plated onto selective LB agar plates (carbenicillin) overnight at 37 °C. A single colony was used to inoculate a 30 mL starter culture in LB Broth with carbenicillin and grown at 37 °C overnight. The next day, this starter culture was used to inoculate 1 L LB Broth with carbenicillin and grown, with agitation, at 37 °C. When cells reached an optical density (OD₆₀₀) of 0.7, protein expression was induced with 0.5 mM isopropyl β-D-1-thiogalactopyranoside (IPTG) and cells were shaken for an additional 15 h at 18 °C. Cell pellets were collected by centrifugation, flash-frozen and stored at -80 °C as previously detailed (Okesli-Armlovich et al., 2019).

Pellets were thawed and resuspended in lysis buffer containing Tris (40 mM pH 7.5), NaCl (10 mM), imidazole (10 mM), dithiothreitol (DTT) (1 mM) and glycerol (10% v/v). Cells were lysed by sonication and centrifuged at 25,000g for 1 h. The supernatant was incubated with a slurry of Ni-NTA resin for 1 h at 4 °C prior to column loading. The nickel column wash buffer was identical to lysis buffer with each wash step introducing increasing imidazole concentrations (10 mM, 50 mM, 250 mM). After SDS-PAGE confirmation of protein fractions, the protein was further purified using an Äkta Pure 25 FPLC with a 5 mL Hi Trap Q anion exchange column. Protein was eluted on a linear gradient from FPLC Buffer A (50 mM Tris-HCl pH 8, 1 mM DTT, 10% glycerol) to FPLC buffer B (50 mM Tris-HCl pH 8, 1 mM DTT, 10% glycerol with 500 mM NaCl) from 2% to 100% Buffer B. Eluates containing recombinant UCK2 were concentrated and exchanged into storage buffer (50 mM Tris-HCl pH 7.5, 10% glycerol) using a centrifugal filter with a 3 KDa cut-off (Amicon). Enzyme was aliquoted, flash-frozen and kept at -80 °C.

Purification of Recombinant Human CMPK1

Previously, human CMPK1 was cloned into the pET28 vector resulting in an expression vector for N-terminally 6×His-tagged CMPK1 (Deans et al., 2016). As previously described, *E. coli* BL21(DE3) cells were transformed with this pET28-CMPK1 expression plasmid, and single colony transformants were used to inoculate a 5 mL starter culture in LB Broth with kanamycin and grown at 37 °C overnight. The next day, this starter culture was used to inoculate 1 L LB Broth with kanamycin and grown, with agitation, at 37 °C until an OD₆₀₀ of ~0.65 was reached (Deans et al., 2016). Cell pellets were harvested by centrifugation and stored at -80 °C (Deans et al., 2016).

Pellets were thawed and resuspended in lysis buffer containing Tris (40 mM pH 7.5), NaCl (10 mM), NaF (5 mM) and DTT (1 mM). Cells were lysed by sonication and supernatant was clarified at 25,000g for 1 h. This supernatant was incubated with a slurry of Ni-NTA resin for 1 h at 4 °C prior to column loading. The nickel column wash buffer was identical to the lysis buffer with each wash step introducing increasing imidazole (0 mM, 10 mM, 40 mM, 200 mM) (Deans et al., 2016). After confirming Ni-NTA wash eluates by SDS-PAGE, relevant protein fractions were diluted as needed, in FPLC Buffer AA (50 mM Tris-HCl pH 8.0, 1 mM DTT) as previously detailed (Deans et al., 2016). The protein was further purified using an Äkta Pure 25 FPLC with a Hi Trap Q anion exchange column. Protein was eluted using a linear gradient from 0 to 95% FPLC Buffer BB (50 mM Tris-HCl pH 8.0, 1 mM DTT, 500 mM NaCl) under established conditions (Deans et al., 2016). Fractions containing CMPK1 were concentrated and exchanged into storage buffer (50 mM Tris-HCl pH 7.5, 10% glycerol) using a 10 kDa filter as previously detailed (Deans et al., 2016). Enzyme was then aliquoted, flash-frozen and kept at -80 °C.

In Vitro Enzyme Activity Assays with UCK2

To continuously monitor reaction progress spectrophotometrically, ATP hydrolysis was coupled to NADH oxidation via pyruvate kinase (PK) and lactate dehydrogenase (LDH) (Tomoike et al., 2017). Reactions were conducted at room temperature in 100 μL in 96-well plates (Greiner Bio-One, UV-Star, Half Area). Mixtures contained 20 mM HEPES pH 7.2, 100 mM KCl, 2 mM MgCl₂, 300 μM ATP, 0-500 μM uridine, 0-500 μM CPU analogs, 10 nM UCK2 (unless otherwise noted), 1 mM phosphoenolpyruvate, 500 μM NADH and 20 units/mL of PK and LDH. Progress was monitored in the linear region using a Biotek Synergy HT and kinetic and inhibition constants were determined using GraphPad Prism.

Enzymatic Synthesis of CMP, CPU-MP, and 5-F-CPU-MP

Reactions were conducted at room temperature in 100 μL in Eppendorf tubes. Mixtures contained 20 mM HEPES pH 7.2, 100 mM KCl, 2 mM MgCl₂, 2.5 mM ATP, 5 mM substrates (cytidine, CPU and 5-F-CPU), and 2 μM UCK2. After gently mixing for 24 h on a

rocking shaker, the reaction mixtures were heated for 3 minutes at 95 °C to denature the UCK2 enzyme. Formation of CPU-MP and 5-F-CPU-MP were confirmed by LC-MS/MS (Figure S1).

In Vitro Enzyme Activity Assays with CMPK1

In a similar manner as the UCK2 assay, ATP hydrolysis was coupled to NADH oxidation via PK and LDH to continuously monitor reaction progress spectrophotometrically. Reactions were conducted at room temperature in 50 μ L in 96-well plates (Greiner Bio-One, UV-Star, Half Area). The CMPK1 assay buffer contained 50 mM Tris-HCl pH 7.5, 50 mM KCl, 5 mM MgCl₂, 2 mM DTT, 500 μ M NADH, 1 mM PEP and 20 units/mL of PK and LDH. To 39.5 μ L of CMPK1 assay buffer, 5 μ L were added of 0–1 mM stock solutions of substrates (CMP from the commercial vendor and denatured UCK2 reaction mixtures containing newly synthesized CMP, CPU-MP and 5-F-CPU-MP) in UCK2 assay buffer. After UV-readouts at 340 nm stabilized (\sim 5 minutes), a mixture of ATP and CMPK1 in CMPK1 assay buffer was added to a final reaction volume of 50 μ L, a final ATP concentration of 500 μ M and a final CMPK1 concentration of 20–100 nM. Progress was monitored in the linear region using a Biotek Synergy HT, and kinetic constants were determined using GraphPad Prism. Generation of CPU-DP and 5-F-CPU-DP was confirmed by LC-MS/MS (Figure S2).

Sample Preparation for LC-MS/MS Analysis

A549 cells were plated overnight at 80,000 cells/well in 24-well plates in complete DMEM. The next day, cells were treated with dipyrindamole or 250 μ M or 500 μ M CPU, 5-F-CPU or 5'-F-CPU in DMEM additionally supplemented with 1 μ M GSK983 and 5 μ M uridine. Six or twelve hours after drug addition, the cell culture medium was removed and the whole plate was rapidly rinsed twice by dipping vertically into a beaker containing 37 °C Milli-Q water. The plate was then placed on dry ice, followed by the addition of 0.5 mL -20 °C lysis buffer (MeCN:MeOH:H₂O = 2:2:1) containing 0.5 M formic acid and 450 nM uridine ¹⁵N₂ monophosphate sodium salt (Sigma Aldrich). The solution was then sonicated for 3 \times 5 minutes on ice for the metabolite extraction. Subsequently, the sample was frozen with liquid nitrogen, freeze-dried, re-suspended with 150 μ L Milli-Q water, and finally filtered through a MultiScreen 96-well filter plate prior to LC-MS analysis.

LC-MS/MS Analysis

LC-MS/MS was performed on an Agilent 1290 infinity II LC system tandem with 6470 triple quad mass spectrometer using ion pairing chromatography. LC separation was performed at 40 °C with a solvent flow rate of 0.25 mL/min on a Zorbax RRHD Extended-C18 column (2.1 \times 150 mm, 1.8 μ m). Buffer A contained 97% H₂O, 3% MeOH, 5 mM tributylamine, 5.5 mM Acetic acid and 1 μ M medronic acid with pH=5.0. Buffer B contains ca. 100% MeOH, 5 mM tributylamine, 5.5 mM acetic acid and 10 μ M medronic acid with pH = 7.0. The initial mobile phase composition was 100% solvent A, and the gradient (%B) after sample injection was as follows: 0% at 2.5 min, 20% at 7.5 min, 45% at 14 min, 99% at 20 to 23 min, and 0% from 23.1 to 27.1 min. The autosampler temperature was set to 4 °C and the sample was injected at 5 μ L. Samples were measured in the negative ESI mode with capillary voltage at -3.5 kV. Further source settings were as follows: gas temperature, 250 °C; gas flow, 13 L/min; nebulizer, 35 psi; sheath gas temperature, 325 °C; sheath gas flow, 12 L/min; nozzle voltage, 500 V; and delta EMV, -200 . Acquisition was performed in dynamic multiple reaction monitoring (dMRM) mode with fragmentation pattern and retention time setting as Table S1.

DENV-2 Luciferase Reporter Assays

A549 cells were plated overnight at 5,000 cells/well in 96-well plates in complete DMEM and incubated for 24 h at 37 °C. Cells were then treated with pyrimidine *de novo* synthesis inhibitors, and/or salvage inhibitors, and/or R1479 in DMEM supplemented with 20 μ M uridine. Four hours after drug addition, cells were infected with DENV-2 virus at a MOI = 0.04. After 48 h or 72 h, DENV-Luc replication was monitored by the production of Renilla luciferase, which was measured using the Renilla-Glo Luciferase Assay System (Promega) according to the specifications of the manufacturer.

For the accompanying cell viability assay, A549 cells were seeded at 5,000 cells/well in 96-well plates in complete DMEM and incubated for 24 h at 37 °C. Cell were then treated with pyrimidine *de novo* synthesis inhibitors, and/or salvage inhibitors, and/or R1479 in DMEM supplemented with 20 μ M uridine. Following 48 h or 72 h treatment, cell viability was monitored via ATP levels, which were measured using the CellTiter-Glo Luciferase Assay System (Promega) according to the specifications of the manufacturer.

For viral tests of the CPU-GSK983 combination (Figure 5B), A549 cells were plated overnight at 20,000 cells/well in 24-well plates in complete DMEM and incubated for 24 h at 37 °C. Cell were then treated with pyrimidine *de novo* synthesis and/or salvage inhibitors in DMEM supplemented with 20 μ M uridine. Four hours after drug addition, cells were infected with the DENV-2 virus infectious clone at a MOI = 0.01. After 48 h, DENV-Luc replication was monitored by the production of Renilla luciferase, which was measured using the Renilla-Glo Luciferase Assay System (Promega) according to the specifications of the manufacturer.

For cell viability tests of the CPU-GSK983 combination (Figure 5B), A549 cells were seeded into 24-well plates at a density of 20,000 cells/well incubated for 24 h at 37 °C. Cell were then treated with pyrimidine *de novo* synthesis and/or salvage inhibitors in DMEM supplemented with 20 μ M uridine. Following 48 h treatment, cells were harvested, and the density of viable cells was determined by flow cytometry (FSC/SSC) using a BD Accuri C6 Flow Cytometer.

Replicon Assays

A549 cells transfected with the pDENV-Luc replicon were plated at 15,000 cells/well in 96-well plates, and immediately treated with R1479, and/or, pyrimidine *de novo* synthesis inhibitors, and/or salvage inhibitors in complete DMEM medium supplemented with

20 μ M uridine without antibiotics (Marceau et al, 2016). Forty-eight hours after drug treatment, cells were lysed and subjected to Renilla luciferase detection, which was measured using the Renilla-Glo Luciferase Assay System (Promega) according to the specifications of the manufacturer.

QUANTIFICATION AND STATISTICAL ANALYSIS

Statistical analyses were performed using GraphPad Prism. In Figure 3, kinetic constants were calculated using this software. In Figures 4A, 5A, and S4, comparisons to an untreated control were calculated using one-way ANOVA, Dunnett's test as detailed in Figure legends. In Figures 5B, 6, 7, S5, and S6, the IC_{50} curves visualized and IC_{50} values provided were generated using a non-linear fit (variable slope, four parameters, constrained to positive values). Additional experimental conditions are detailed in Figure captions.